

Recent progress of Ga₂O₃-based gas sensors

Hongchao Zhai, Zhengyuan Wu ^{*}, Zhilai Fang ^{**}

Academy for Engineering & Technology, School of Information Science and Technology, Fudan University, Shanghai, 200433, China



ARTICLE INFO

Keywords:

Gallium oxide
Gas sensors
Gas sensing mechanism
Response
Selectivity

ABSTRACT

In recent years, gas sensors fabricated from gallium oxide (Ga₂O₃) materials have aroused intense research interest due to the superior material properties of large dielectric constant, good thermal and chemical stability, excellent electrical properties, and good gas sensing. Over the past decades, Ga₂O₃-based gas sensors experienced rapid development. The long-term stable Ga₂O₃-based gas sensors for detecting oxygen and carbon monoxide have been commercialized and renowned with extremely good gas sensing characteristics. Recent pioneering studies also exhibit that the Ga₂O₃-based gas sensors possess great potentials in applications of detecting nitrogen oxides, hydrogen, volatile organic compounds and ammonia gases. This article presents recent advances in gas sensing mechanism, device performance parameters, influence factors, and applications of Ga₂O₃-based gas sensors. The impacts of influence factors, doping, material structure and device structure on the performance of gas sensors are discussed in detail. Finally, a brief overview of challenges and opportunities for the Ga₂O₃-based gas sensors is presented.

1. Introduction

The rapid development of science and technology has brought great convenience to our life, but also left a lot of problems, among which the serious air pollution affects the health of human body and also causes environmental problems such as the greenhouse effect, smog, acid rain, ozone hole, etc. Incomplete combustion of fuels in industrial production and vehicle causes not only the environmental problems but also the loss of energy. According to a United States Department of Energy report, harsh environment sensors are predicted to save 0.25 quadrillion BTU/year of energy across all energy-consuming industries [1]. In industrial production and laboratory research, with the full understanding and using of toxic, harmful, flammable and explosive gases, the detection of gas leaks is necessary. In the medical treatment and the new health examination, the breath examination of human body is also an important part. Therefore, the development of gas sensor with high response, fast response speed, high stability, low detection limit and high selectivity is an important task of all the recent scientific researches.

The emergence of sensors derives from the first pioneering attempts with electrochemical-sensing glass electrode and Heyrovsky's invention of polarography [2–5]. With the equipment update, material development and theoretical breakthrough, scientists have gradually developed applications in gas sensing. Gas sensors are divided into electrochemical

gas sensors, catalytic combustion gas sensors, thermal conductivity gas sensors, infrared gas sensors, solid electrolyte gas sensors and semiconductor gas sensors, etc. In recent two decades, semiconductor gas sensors have attracted great attention due to its merits of fast response speed, easy manufacturing, good repeatability, low cost and good compatibility in integrated circuits, and good gas sensitivity on the surface of oxide semiconductors. The SnO₂ semiconductor gas sensors are firstly commercialized but lack of the selectivity [6]. High-performance oxide semiconductor gas sensors are also fabricated on some oxides materials, such as ZnO, In₂O₃, TiO₂, WO₃, etc. [7–11]. Recently, some oxide semiconductor gas sensors based on NiO, CuO, Co₃O₄, Cr₂O₃, Mn₃O₄, La₂O₃, Ga₂O₃ also attract great attention [12–16]. In these studies, different gas-sensing properties have been found in these oxide semiconductors and facilitate the exploration of new functionalities of oxide semiconductor gas sensors. Interestingly, the size and doping of the material can modulate the material properties and lead to the emergence of novel physical and chemical properties. The oxide semiconductors show a great potential in gas sensors.

Ga₂O₃ is an ultrawide-bandgap semiconductor material that has attracted much attention in recent years. Ga₂O₃ has five polymorphs, namely α , β , γ , δ and ϵ , among which β phase is the most stable structure, and other phases will convert to β phase when heated to 1000 °C or above 300 °C by wet method. β -Ga₂O₃ has a bandgap of 4.9 eV, a

* Corresponding author.

** Corresponding author.

E-mail addresses: zhengyuanwu@fudan.edu.cn (Z. Wu), zlfang@fudan.edu.cn (Z. Fang).

breakdown field of 8 MV/cm, a dielectric constant of 10, a Baliga's figure of merits of 3444 and good thermal and chemical stability [17–25], making it an appropriate candidate for power electronic devices, optoelectronic devices and gas sensors. With the improvement of the crystal quality of Ga_2O_3 film and nanostructure materials in recent years, the solar-blind ultraviolet (UV) detectors [21,22] and power electronic devices [23,24] based on these materials have shown excellent performance, and gas sensors based on high-quality Ga_2O_3 materials also attract more attention due to good gas sensing [16]. Great efforts have been made to improve the performance, response to oxidizing gases, and selectivity of Ga_2O_3 -based gas sensors by intentional doping, spill-over effect, UV illumination, formation of core-shell structure or nanostructure or heterojunction film, and device structure optimization. Intensive studies of sensing mechanism are needed to further understand and improve the performance of the Ga_2O_3 -based gas sensors.

In this review, we introduce the sensing mechanism and performance parameters of general gas sensors to give a basic understanding. Then, the influence factors of Ga_2O_3 -based gas sensors are given, which is key for the performance of gas sensors. Finally, we review the applications of Ga_2O_3 -based gas sensors in detection of oxygen (O_2), carbon monoxide (CO), nitrogen oxides (NO_x), hydrogen (H_2), and other gas, and summarize some performance enhancement methods, such as doping, nanostructure, core-shell structure, heterojunction film or nanostructure, spill-over effect, UV illumination, and device structure optimization. Challenges and opportunities for the Ga_2O_3 -based gas sensors are also discussed.

2. Gas sensing mechanism

The gas sensing of semiconductor sensors is based on the monitor of the change in conductivity induced by the target gas. In order to explain the mechanism of this gas sensing phenomenon, many theories have been proposed and summarized mainly as adsorption/desorption model and surface depletion layer theory [26].

The adsorption/desorption model is the basis of the most current mainstream gas sensing mechanisms, and proposed based on the discovery of bulk conductance effects, which is a variation in the conductivity and work function (associated with surface depletion layer) of materials under the change in the surrounding atmosphere. When the sensor is exposed to target gas, the adsorption/desorption of the gas molecules on the surface of a material will occur and thus induce a reaction involving the gas molecules ionization to transfer electrons or holes between sensor surface and target gas. The carrier transfer can change the density of charge carriers available in sensors and then vary the conductivity of sensors progressively. The relationship between gas sensing parameters (such as the operating temperature, target gas partial pressure, gas absorption capacity, ionic conduction activation energy) and the electrical conductivity of sensor may be represented by Ref. [27]:

$$\sigma = A \exp(-E_A/kT) P_{\text{gas}}^{1/N} \quad (1)$$

where A denotes a constant determined by the basis conductivity of materials, E_A the activation energy for conduction characterizing the ionic conduction process, k the Boltzmann constant, T the temperature, P_{gas} the target gas partial pressure, and N the empirical constant. The parameters of E_A and N are used to calibrate the gap between the actual capacitance and a pure capacitance, and determined by gas absorption capacity and adsorbed gas ionic conduction efficiency of materials. The activation energy is significantly involved with the sensor sensitivity and the operation temperature of the gas sensors. For example, the decrease of activation energy of target gas adsorption indicates the enhancement of the sensor sensitivity, and also implies a shift of the temperature-dependent response peak for gas sensors [28]. The operation temperature is another important parameter. The sensitivity of Ga_2O_3 gas

sensors increases with the operation temperature based on Equation (1). High thermal stability and strong gas sensing at high temperature (HT) make Ga_2O_3 as an appropriate candidate for HT gas sensors.

In air atmosphere, oxygen molecules are usually chemisorbed on the surfaces of gas sensors spontaneously before detecting the target gas, and then converted to oxygen ions including O_2^- , O^- and O^{2-} by the reaction, which is summarized below:



The aforementioned reaction can consume electrons to induce a variation of the charge depletion region on the semiconductor surface, as shown in Fig. 1 [29]. This variation of the charge depletion region before detecting the target gas will make the calculation [based on Equation (1)] of the target-gas-induced conductivity change inaccurate. Therefore, the surface depletion layer theory, which is a theoretical concept based on the adsorption/desorption model, is employed to deeply analyze the gas sensing mechanism in the atmospheric environment. During the gas sensing, the exchange of carriers at the surface of the sensor will induce a charge depletion region, which is called as the surface depletion layer. For the semiconductor device, the charge depletion region has a width. The variation of the width of charge depletion region will change the conductivity of the gas sensor. Based on drift-diffusion theory, the width of charge depletion region (x_{dep}) can be deduced as [30]:

$$x_{\text{dep}} = (2eV_{\text{sur}}/eN_i)^{1/2} \quad (5)$$

where ϵ denotes the permittivity of materials, V_{sur} the potential barrier at the surface, N_i the concentration of ionized impurities in the material, e the electron charge.

This equation shows that the width of depletion region is determined by physical properties of materials and the surface potential barrier (V_{sur}). The width of charge depletion region can be used to derive the Debye length to evaluate the limit of gas-sensing electrical signal. When the thickness of the material is less than twice the Debye length, the surface depletion layer will extend to the entire material. The change of electrical signal in gas sensor will reach the maximum.

The potential barrier (V_{sur}) is caused by the adsorption of target gas depending on the relative values (i.e. the adsorption/desorption between oxygen and target gas), and can be deduced from Refs. [31,32]:

$$dV_{\text{sur}}/dx = -eN_{\text{absorbed}}/\epsilon \quad (6)$$

where e denotes the electron charge, N_{absorbed} the density of the actual adsorbed molecules (i.e. gas absorption capacity), ϵ the permittivity of materials.

Based on integrating Poisson equation, the electrical conductivity of sensor under equilibrium is given by Ref. [33]:

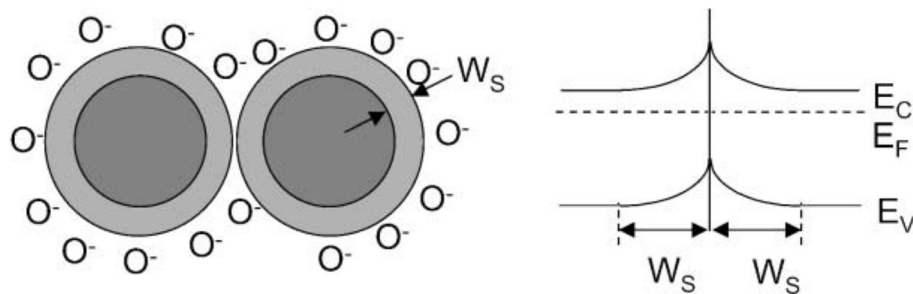
$$\sigma = \sigma_0 \times \exp(-e\Delta V_{\text{sur}}/kT) \quad (7)$$

where σ_0 denotes the basis conductivity of materials, ΔV_{sur} the shift of the potential barrier at the surface.

The target gases usually act as either oxidizing or reducing agents. Due to this different nature of target gas, the gas sensing mechanism of the surface depletion layer theory is divided into oxidizing gas sensing mechanism and reducing gas sensing mechanism. The NO_x gas is the oxidizing gas with some similar properties as oxygen. When NO_x is exposed to an n-type gas sensor, it will capture electrons from sensors or react with oxygen ions at surface of sensors, based on the following reaction:



(a) Oxidizing gases (e.g. O₂) atmosphere



(b) Reducing gases (e.g. CO) atmosphere

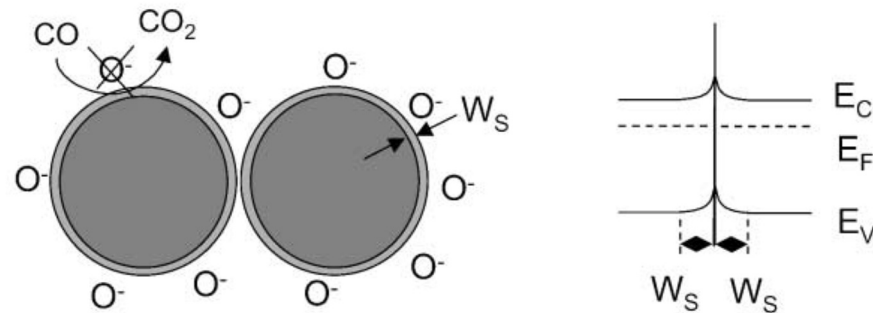
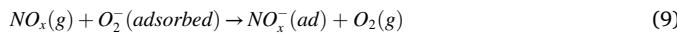
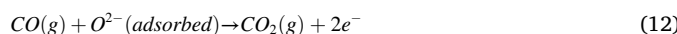
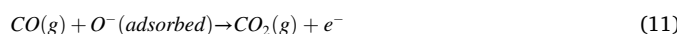
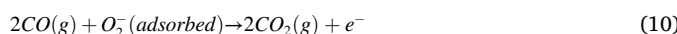


Fig. 1. Gas sensing mechanisms of n-type gas sensors interpreted by surface model and band model in (a) oxidizing gases atmosphere, and (b) reducing gases atmosphere. (a) and (b) Adapted with permission [29]. Copyright 2001, Elsevier.



The loss of electrons in sensors will widen the width of charge depletion region leading to the increase of its resistance (Fig. 1a), indicating that oxidizing target gas will increase the resistance of n-type gas sensors.

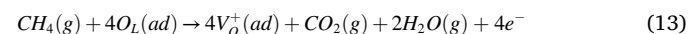
The reaction between the reducing gas and the sensor is opposite to that between the oxidizing gas and the sensor. When a reducing gas such as CO is exposed to an n-type gas sensor, it will react with the chemisorbed oxygen ions and then release electrons, based on the chemical reaction:



The increase of electrons in sensors will decrease the width of depletion layer to decrease of its resistance (Fig. 1b), indicating that reducing target gas will decrease the resistance of n-type gas sensors. In p-type gas sensors, the process involves the abstraction of holes from surface of sensors. The gas sensing phenomena exhibited by the p-type gas sensors exposed into reducing and oxidizing gases are opposite to those exhibited by n-type gas sensors. The variation of the resistance in

n-type or p-type gas sensors exposed to reducing and oxidizing gases is summarized in Table 1.

In recent years, many novel gas sensing mechanisms and phenomena have been discovered and proposed. Hoefer et al. consider that the lattice oxygen vacancy will be formed in oxide semiconductor materials, due to a reaction between the target gas and the lattice oxygen at HT (>800 °C), to release electrons in the crystal (Fig. 2a) [29]. The reaction process is written below:



In porous oxides, the gas sensing mechanism at operation temperature above 260 °C is based on porous-size-related gas diffusion instead of the surface chemical adsorption/desorption [34]. The sensitivity and response speed are determined by the gas diffusion length and the Knudsen diffusion coefficient. The gas sensing mechanism of CO, H₂, hydrogen sulfide (H₂S), etc. gas sensors fabricated from some oxides (e.g. γ-Fe₂O₃ and WO₃, CuO, etc.) is based on the surface structural phase transformation instead of the surface depletion layer variation [35–40], as shown in Fig. 2b. The oxides gas sensors based on the phase transformation mechanism usually suffer from a significant response fluctuation. Some quasiparticles (e.g. interlayer excitons) in oxides van-der-Waals heterostructures are also employed to enhance the gas absorption of oxides [41], as shown in Fig. 2c. Recently, strong gas adsorption/desorption phenomena are observed in the hydrogen and hydride gas sensing of some sesquioxides (Ga₂O₃, Ho₂O₃, etc.) due to a special O–H configuration [42].

3. Performance parameters

The basic parameters such as response (*S*), response and recovery time (*τ*), selectivity and linearity (*γ_L*) have been defined to evaluate the performance of gas sensors. Details of these parameters are described as follows:

Table 1

The resistance response of n-type or p-type gas sensor to the introduction of reducing or oxidizing gases into an air ambient.

Characteristic of surface depletion layer	Oxidizing gases	Reducing gases
n-type	Increase of resistance	Decrease of resistance
p-type	Decrease of resistance	Increase of resistance

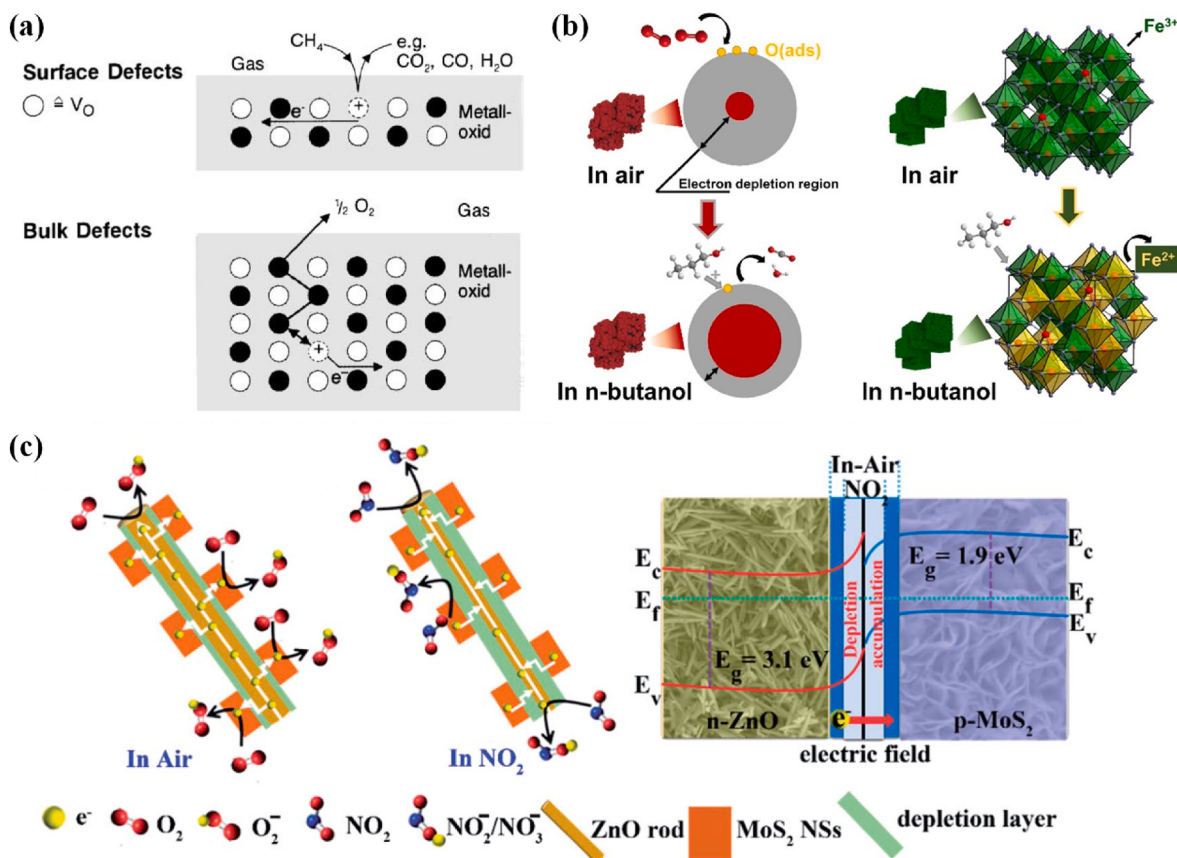


Fig. 2. (a) Gas sensing mechanism interpreted by the lattice oxygen vacancy mode for oxide semiconductor at HT (>800 °C) showing the formation process of the surface oxygen vacancy and the bulk oxygen vacancy. (b) Gas sensing mechanism interpreted by the surface structural phase transformation for Fe₂O₃-based gas sensors exposed to butanol. (c) Gas sensing mechanism interpreted by quasiparticles for some oxides-heterostructures gas sensors. Adapted with permission [29]. Copyright 2001, Elsevier. (b) Adapted with permission [40]. Copyright 2019, Elsevier. (c) Adapted with permission [41]. Copyright 2021, The Royal Society of Chemistry.

3.1. Response

The response is applied to characterize the change of resistance in gas sensor and defined by the ratio of basis conductivity to the change of conductivity in gas sensors. There are three calculation methods to estimate the response of the sensor exposed to reducing gases, which can be obtained by formulas $S_1 = R_a/R_g$, $S_2 = \Delta R/R_g$, $S_3(\%) = (\Delta R/R_a) \times 100\%$, where S denotes the response, R_a the resistance in air, R_g the resistance in target gas, $\Delta R = |R_g - R_a|$ the resistance change value. Based on chemical formulas (7) – (11), the resistance change of the sensor in oxidizing gases is opposite to that of the sensor in reducing gases. The response of the gas sensor in oxidizing gases is obtained by formulas $S_1 = R_g/R_a$, $S_2 = \Delta R/R_a$, $S_3(\%) = (\Delta R/R_g) \times 100\%$. We can read R_a and R_g , which is defined as the resistance at the time of gas “on” and gas “off” shown in Fig. 3a, and calculate response through the above-mentioned methods. Different calculation methods lead to different response value. When using method S_1 and S_3 , the former response value is more than 1 and the latter response value ranges from 0% to 100%. In this review, a uniform standard S_1 will be used to compare different experimental data. The response of the gas sensor is usually determined by the width of depletion region (limited by the Debye length) and thus influenced by the permittivity, doping concentration of materials, and the density of the actual adsorbed molecules.

3.2. Response and recovery time

The response time and recovery time are important performance parameters to evaluate response speed of gas sensors. Response time is

defined as the time consumed to reach 90% of resistance change value in target gas, and recovery time is given by the time consumed to return 90% of the resistance change value in air. As shown in Fig. 3a, the response time is given by $\tau_{res} = \tau_2 - \tau_1$, where, τ_1 denotes the time when the target gas is sensed, τ_2 the time when the resistance changes at R_{res} ($R_{res} = R_a - 90\% \times \Delta R$). Correspondingly, the recovery time is given by $\tau_{rec} = \tau_4 - \tau_3$, where, τ_3 the time when the target gas is removed, τ_4 the time when the resistance changes at R_{rec} ($R_{rec} = R_g + 90\% \times \Delta R$). The response time and recovery time of most gas sensors fabricated on various materials is too long due to slow gas absorption/desorption rate and carrier diffusion-equilibration rate. The Ga₂O₃-based gas sensors with short response time and recovery time are essential for the rapid detection of the target gas and need to be developed. Currently, the fabrication of fast-response gas sensors is still a challenge.

3.3. Selectivity

The selectivity is an ability of a gas sensor to detect a specific gas in the gas mixture, and determined by the carrier concentration and gas absorption capacity of materials based on Equations (5) and (6). A good selectivity of gas sensor is necessary for their commercialization. Unfortunately, the material of the gas sensor is usually sensitive to many gases and thus some undesirable interference signals will be produced during detecting (Fig. 3b) [43], which makes a great challenge to achieve good selectivity. Based on Equation (6), one approach by modulating the gas absorption capacity of materials has been proposed to improve the selectivity and consists of interface modification technique, operating temperature modulation, nanostructure, heterostructure, and

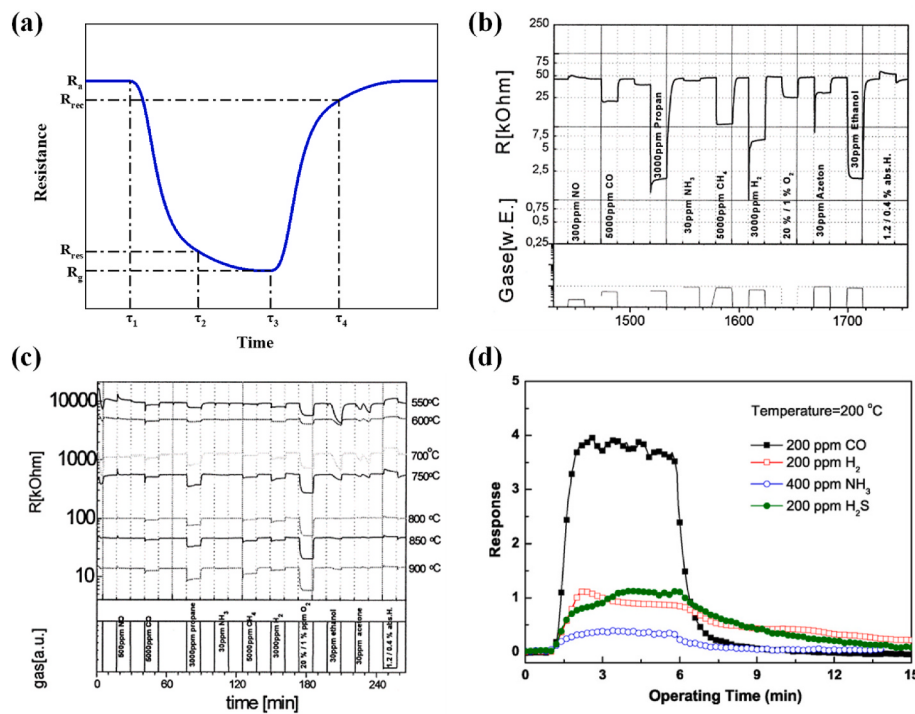


Fig. 3. (a) A typical response curve of n-type oxide semiconductor gas sensor to reducing gases. Sensor-resistance of pure and modified sensors at different temperatures: (b) unmodified and (c) La₂O₃ modified. (d) Responses of the Ga₂O₃ nanowire sensor exposed to 200 ppm CO, 200 ppm H₂, 400 ppm NH₃, and 200 ppm H₂S at 200 °C. (b) and (c) Adapted with permission [43]. Copyright 2000, Elsevier. (d) Adapted with permission [44]. Copyright 2008, Elsevier.

so on. For example, the selective O₂ detection of Ga₂O₃-film gas sensor can be enhanced by the modulation of the gas absorption capacity via the interface modification (Fig. 3c) [43]. The gas sensor fabricated on Ga₂O₃ nanowire exhibits the well selective CO detection (Fig. 3d) [44]. Another approach to enhance the selectivity is to promote a certain electrochemical reaction in gas sensors by modulating impurity doping or adding the polarization voltage to modulate the carrier concentration.

3.4. Linearity

The linearity of gas sensors displays the linear response of the device to target gas concentration. Good linear sensing characteristics are beneficial to theoretical analysis, design calculation, measuring calibration and data processing, and indicate the reliability of detecting target gas. The linearity is defined by the quantitative index $r_L = \frac{\Delta L_{max}}{y_{FS}} \times 100\%$, where ΔL_{max} denotes the maximum deviation, y_{FS} the output value at full scale. The linearity quantitative index also can be obtained

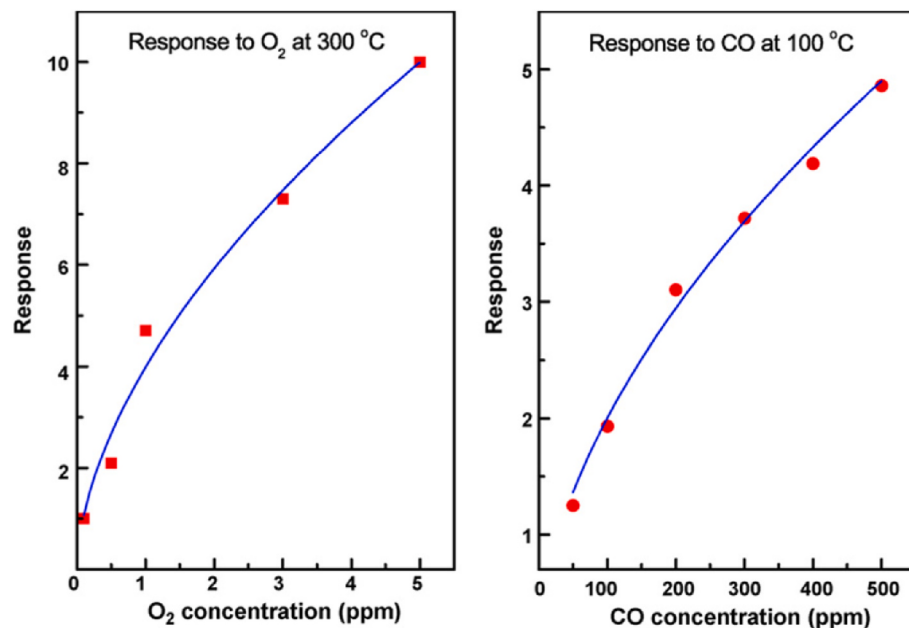


Fig. 4. Concentration dependence of the response to O₂ and CO. Adapted with permission [44]. Copyright 2008, Elsevier.

by an empirical equation about the relationship between the response and the target gas concentration, $S = aC^b$, where C is the target gas concentration, a the constant related to the target gas, b the linearity quantitative index [44]. Based on this empirical equation, we can fit the curve of concentration dependence of the response to target gas to obtain the linearity quantitative index. As shown in Fig. 4, the curve of concentration dependence of the response to O₂ and CO is fitted using the empirical equation. The linearity quantitative index is between 0.35 and 1.00, and can be influenced by operation temperature and applied bias voltage. In general, the linearity quantitative index needs to be optimized to 1. In addition, there are response saturation and limits of detection (LOD) for gas sensors. The response saturation, which is correlated with Debye length and roughly estimated by Equation (6), occurs at the gas concentration typically of 10⁴–10⁵ ppm for the Ga₂O₃ gas sensors [45]. The LOD, which is influenced by the activation energy (E_A), gas absorption capacity, adsorbed gas ionic conduction efficiency and so on, is about 10⁻²–10⁻¹ ppm for the Ga₂O₃ gas sensors [46–48].

4. Influence factors

4.1. Temperature

The operation temperature has a significant impact on the resistance of gas sensors based on Equation (1) and has different impacts on gas sensitivity for different gases. The response of Ga₂O₃ gas sensors to some gases possesses obvious temperature sensitivity. For example, the response to hydrogen peaks at 675 °C and the response of methane peaks at 825 °C, while the response to other gases has no significant changes, as shown in Fig. 5a [49]. Frank et al. studied the temperature dependences of sensitivity to methane, isobutene and carbon monoxide for pure and Sn-doped Ga₂O₃ thin films gas sensors [50]. An obvious change in temperature sensitivity to methane whereas no significant changes for the temperature sensitivity to isobutene and carbon monoxide were observed for the Sn-doped Ga₂O₃ thin films gas sensors (Fig. 5b–d). Thus, controlling the operating temperature of gas sensors may enhance selectivity to the target gas and other means like doping may further

monitor selectivity. Nakagomi et al. fabricated a Ga₂O₃-based H₂ gas sensor with self-compensation to solve the performance fluctuation caused by temperature.

4.2. Humidity

Humidity has a negative impact on the performance of gas sensors, because H₂O will occupy adsorption sites and thus prevent gas sensors from adsorbing the target gases. If a gas sensor has a strong humidity effect, a small humidity variation will lead to a large fluctuation in resistance. Therefore, the humidity effect of gas sensors should be minimized during detection. Hoefer et al. studied the relationship between resistance and humidity of commercially available SnO₂-film gas sensor and Ga₂O₃-film gas sensor. In range of relative humidity (RH) 30–70%, the resistance fluctuation of Ga₂O₃-based gas sensor is much smaller than that of SnO₂ gas sensor (Fig. 6a), indicating that Ga₂O₃ gas sensor is more stable in that humidity range [29]. The Ga₂O₃-nanowire gas sensor also shows weak humidity effect in the range of RH 30–70% [51]. The resistance and the current of the Ga₂O₃-nanowire gas sensor change rapidly in range of RH 70–95% (Fig. 6), indicating a considerable humidity effect at high RH. The strong humidity effect at high RH will cause performance degradation of Ga₂O₃-based gas sensors, and requires to be eliminated.

4.3. UV illumination

In the field of Ga₂O₃ gas sensors, UV illumination can be employed to enhance the response and reduce the response time and recovery time. Fast oxygen response in individual Ga₂O₃ nanowire is observed under the UV illumination condition and attributed to the optically-driven enhancement of oxygen sensing [52]. As shown in Fig. 7a, the UV illumination rapid increase the carrier concentration and thus enhances oxygen adsorption and ionization of the surface of Ga₂O₃ nanowire, resulting in the increase of oxygen response and response speed. The response is usually proportional to UV light power density (Fig. 7b) [53]. For the CO detection, enhancement of gas sensing by UV-illumination is

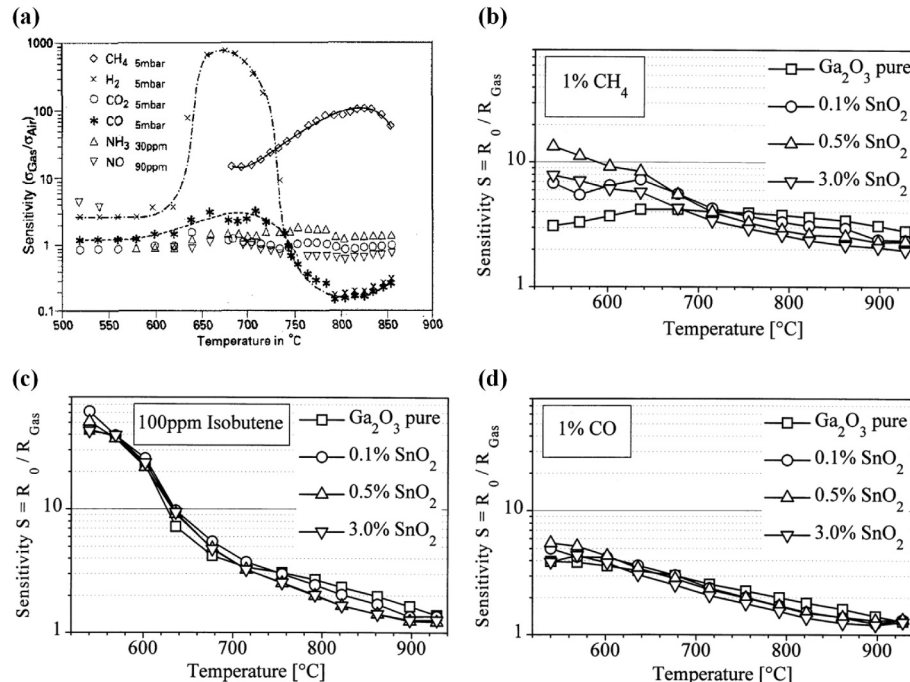


Fig. 5. (a) Temperature dependences of sensitivities of β -Ga₂O₃ thin films to various gases in wet air, and temperature dependences of the sensitivities to (b) 1% CH₄, (c) 100 ppm isobutene and (d) 1% CO for pure and doped Ga₂O₃ thick films in wet air. (a) Adapted with permission [49]. Copyright 1995, Elsevier. (b), (c), and (d) Adapted with permission [50]. Copyright 1998, Elsevier.

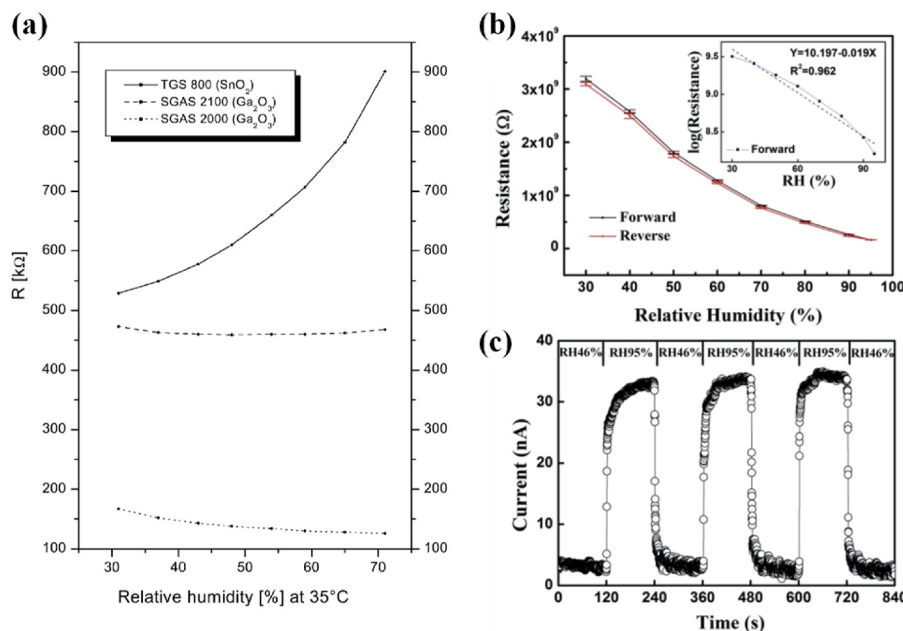


Fig. 6. (a) Variations of resistance with humidity for SnO₂ and Ga₂O₃ gas sensors. (b) Forward and reverse resistance measured in the relative humidity (RH) range between 30 and 95%. Inset is the log resistance as a function of humidity. (c) Dynamic response measured for β-Ga₂O₃ NWs humidity sensor in the RH range between 46 and 95%. (a) Adapted with permission [29]. Copyright 2001, Elsevier. (b) and (c) Adapted with permission [51]. Copyright 2015, The Royal Society of Chemistry.

also observed in the gas sensors fabricated from Ga₂O₃ nanorod, Pt- and La_{0.8}Sr_{0.2}FeO₃(LSFO)-decorated Ga₂O₃ nanorod (Fig. 7c) [54]. The response speed increases after UV illumination on Ga₂O₃ nanorod, Pt- and LSFO-Ga₂O₃ nanorod gas sensors (Fig. 7d). The recovery speed becomes faster after UV illumination on the Ga₂O₃ nanorod gas sensors, whereas the recovery speed becomes slower after UV illumination on the Pt- and LSFO-Ga₂O₃ nanorod gas sensors, indicating an interference between spill-over effect and UV illumination. Further study is required to clarify the origin of the interference between spill-over effect and UV illumination.

5. Applications

In recent years, the excessive burning of fossil fuels has caused the greenhouse effect and other natural disasters, such as photochemical smog, acid rain, eutrophication, ozone hole, etc. Gas sensors play a part in these environmental problems in three processes: source control needs O₂ gas sensors to control oxygen concentration to further improve combustion efficiency; process management needs CO and NO_x gas sensors to detect and treat the exhaust gas emission; alternative solution can use H₂ as an alternative clean energy, but considering its inflammable and explosive properties H₂ gas sensors are needed to monitor H₂ leakage and its concentration. Volatile organic compounds (VOCs), ammonia (NH₃) and ozone are all important industrial and agricultural raw materials which are flammable, explosive or toxic gases, so they need detecting as well.

Equation (5) reveals that due to large dielectric constant Ga₂O₃ has a higher width of depletion layer, compared to that of conventional metal oxide semiconductor materials, which may increase the response to reducing gases of gas sensors. The Ga₂O₃ material has other excellent sensing properties of high thermal and chemical stability, wide operating temperature range, long-term resistance stability, weak humidity influence, etc. The Ga₂O₃ nanostructures can adsorb more oxygen, decrease surface electron density and increase surface potential due to the large surface-to-volume ratio, which will further increase the width of depletion layer according to Equation (5). Therefore, Ga₂O₃-based gas sensors have attracted intense research interest and been extensively studied. In this section, the recent applications of Ga₂O₃ gas sensors for

detecting O₂, CO, NO_x, H₂, and other gases are reviewed. The technologies and mechanisms for improving the gas sensing performance are discussed and concluded. The critical performance parameters of β-Ga₂O₃ gas sensors for O₂, CO, NO_x, H₂, and other gases, respectively, are summarized.

5.1. O₂ gas sensors

The Ga₂O₃ material is one of the best candidates for HT O₂ gas sensors due to its high thermal stability. In 1991, Fleischer et al. reported the pioneering work for the fabrication of HT O₂ gas sensors on polycrystalline Ga₂O₃ thin films with an empirical constant of 1/4 [N, Equation (1)], an activation energy of 1.9 eV [E_A, Equation (1)], a response time of 2–13 s, and a long-term stability (over 150 h) [55,56]. The electrical characteristics revealed that the polycrystalline Ga₂O₃ thin film has a potential application in catalytically inactive oxygen sensors under the condition of suitable temperature compensation. The absence of cross-sensitivity between oxidizing gas (O₂) and reducing gas (CO) also has been observed in this gas sensor operated at 1000 °C, and implies a potential to modulate the selectivity of polycrystalline Ga₂O₃ gas sensor. The crystalline quality of Ga₂O₃ influences the performance of Ga₂O₃ gas sensors at various operation temperature. Bartic et al. have investigated the influence of vacancy-related defects on the performance of β-Ga₂O₃ gas sensors at operation temperature from 700 to 1000 °C [57]. A short response time of 5 s, a maximum response of ~2, and an activation energy of 0.64 eV are observed at 800 °C, while the performance quickly deteriorates and the activation energy increases to 1.37 eV if operated at temperature above 800 °C. The good performance at 800 °C is attributed to the high crystalline quality, remarkable surface reaction, fast surface diffusion and volume diffusion. The deterioration of device performance at high operation temperature (>800 °C) is caused by vacancy-related defects.

Great efforts have been made to improve the response, the response speed, and the selectivity of β-Ga₂O₃ gas sensors. Various methods have been developed including interface modification, doping, nanostructure, UV illumination, and so on. Schwebel et al. sputtered La₂O₃ on the surface of the Ga₂O₃ thin film to suppress gas absorption of the reducing gas for Ga₂O₃ gas sensors, thereby modulating the selectivity of

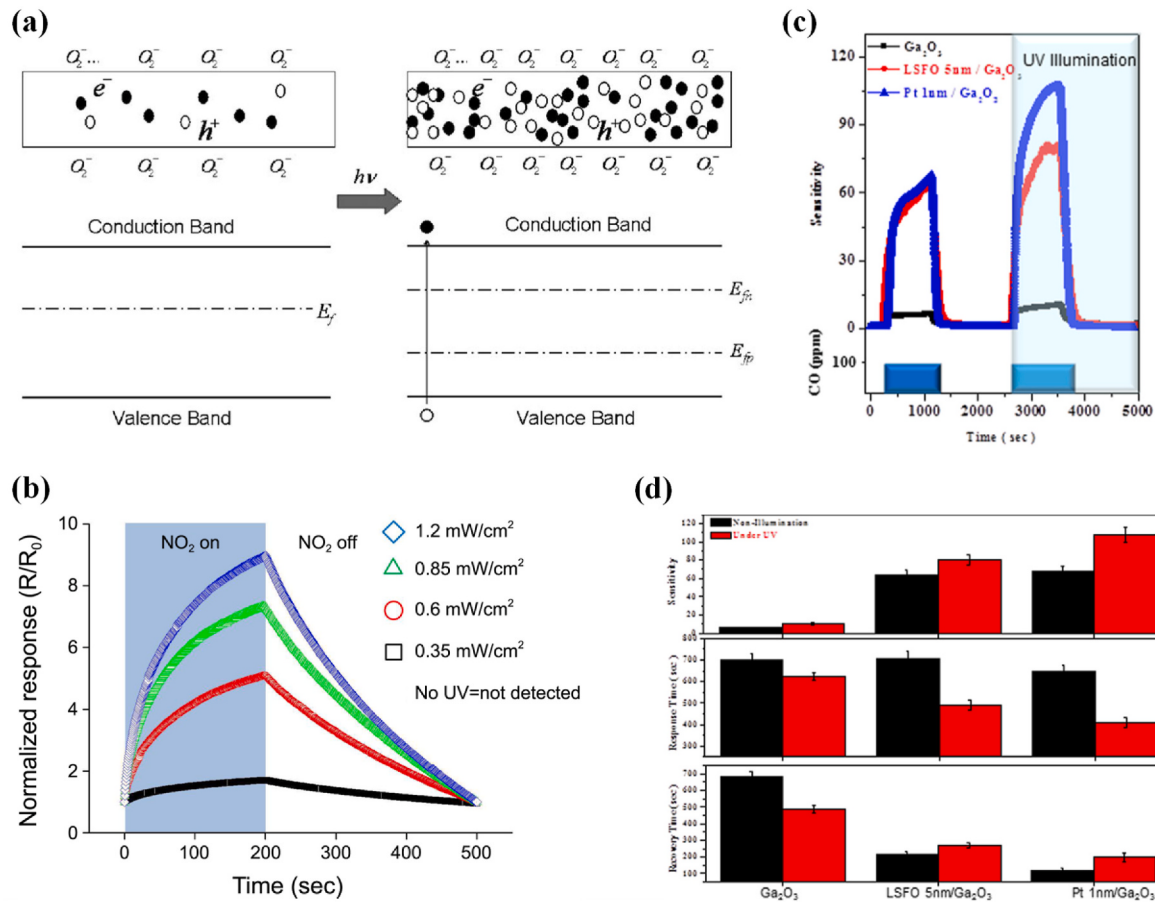


Fig. 7. (a) Schematics and energy-level representations of the $\beta\text{-Ga}_2\text{O}_3$ nanowires before and after the 254 nm UV illumination. (b) Responses of Pt-functionalized Ga_2O_3 nanorod gas sensors exposed to NO_2 gas at 5 ppm with and without UV light illumination. CO gas sensing performance comparison of pristine, LSFO-decorated, and Pt-decorated Ga_2O_3 nanorod arrays: (c) normalized sensitivity-time characteristics and (d) sensitivity, response time, and recovery time under dark or UV illumination tested at 500 °C. (a) Adapted with permission [52]. Copyright 2006, American Institute of Physics. (b) Adapted with permission [53]. Copyright 2013, Wiley Online Library. (c) and (d) Adapted with permission [54]. Copyright 2017, American Institute of Physics.

Ga_2O_3 gas sensors [43]. The pure- Ga_2O_3 thin films gas sensors have a similar response of ~100 to oxidizing gas, reducing gas as well as organic vapors, while the La_2O_3 -modified Ga_2O_3 gas sensors exhibit a reduced response of 1 to reducing gas and organic vapors and a response of 100 to O_2 with an activation energy of 1.6 eV, attributed to suppression of the absorption of reducing gas and organic vapors. The selective detection of Ga_2O_3 -based O_2 gas sensors was improved by the La_2O_3 modification at operation temperature between 750 and 900 °C (Fig. 3c). Li et al. investigated the influences of Ce, Sb, W and Zn dopants on oxygen sensing performance of Ga_2O_3 -film gas sensors [58]. The Ce-doped Ga_2O_3 gas sensors exhibit a response time of 40 s and a recovery time of 30 s, and a response of ~6.45–10000 ppm O_2 at 460 °C. The Zn-doped Ga_2O_3 gas sensors have a long response time of 100 s, a long recovery time of 70 s, and a response of 8–10000 ppm O_2 at 420 °C. The W-doped Ga_2O_3 gas sensors show a long response time of 90 s, a long recovery time of 80 s, and a large response of 56 at 520 °C. The performance of Sb-doped Ga_2O_3 gas sensors is ordinary. Manandhar et al. reported a fast-response 5-at%-Ti-doped Ga_2O_3 -film gas sensor with a response time of ~4 s and attributed it to the improvement of the surface reaction rate and the diffusion rate by Ti dopants [59]. Recent study on Cr-doped $\beta\text{-Ga}_2\text{O}_3$ -film gas sensors shows that the Cr element also acts as catalytically active dopants to improve the oxygen sensing properties of $\beta\text{-Ga}_2\text{O}_3$ [43,60]. The response to oxygen is estimated to be 4–5 with an activation energy of 1.27 eV. The Ga_2O_3 nanomaterials have attracted many attentions due to its high surface-to-volume ratio. In 2008, Liu et al. applied high-quality $\beta\text{-Ga}_2\text{O}_3$ nanowires of monoclinic

structure (Fig. 8a and b) to fabricate gas sensors for both oxygen and carbon monoxide sensing [44]. The $\beta\text{-Ga}_2\text{O}_3$ -nanowires gas sensor has a peak response of 10 to 5% O_2 at 300 °C (Fig. 8c). Feng et al. employed UV illumination on the individual $\beta\text{-Ga}_2\text{O}_3$ nanowire gas sensors to achieve high response and fast response speed [52].

In Table 2, the critical performance parameters of the state-of-the-art Ga_2O_3 -based O_2 gas sensors are summarized [44,57–63]. Since the calculation methods of response are different in these literatures, we employ a standard method of S_1 (pls see section 3.1) to obtain the normalized response for comparisons. According to Equations (5)–(7), the introduction of high-density carrier concentration (i.e. impurities doping) and surface/interface states (e.g. grain boundaries, nanostructure, etc.) is required for the increase of the response [58,64]. Therefore, the normalized response of metal-doped Ga_2O_3 film/nanowire or amorphous Ga_2O_3 gas sensors is significantly higher than that of single-crystal Ga_2O_3 gas sensors. In previous studies, the normalized response of single-crystal Ga_2O_3 gas sensors, metal-doped Ga_2O_3 thin film gas sensors, and Ga_2O_3 nanowires gas sensors is on the order of 0.1, 1, and 10, respectively. In comparison with O_2 gas, the ozone (O_3) has a low activation energy on the surface of Ga_2O_3 -based materials indicating a strong ozone gas sensing at LT due to its intense oxidation reaction [65–68]. A good selectivity of 5–10 is observed above 500 °C for the Ga_2O_3 -based O_2 gas sensors, which is obtained by comparing the response of O_2 , CO , H_2 , NO_x , VOCs, NH_3 , etc. [43,44,60]. The LOD of Ga_2O_3 nanowires gas sensors (10^{-2} ppm) is significantly lower than that of single-crystal Ga_2O_3 gas sensors and Ga_2O_3 thin film sensors

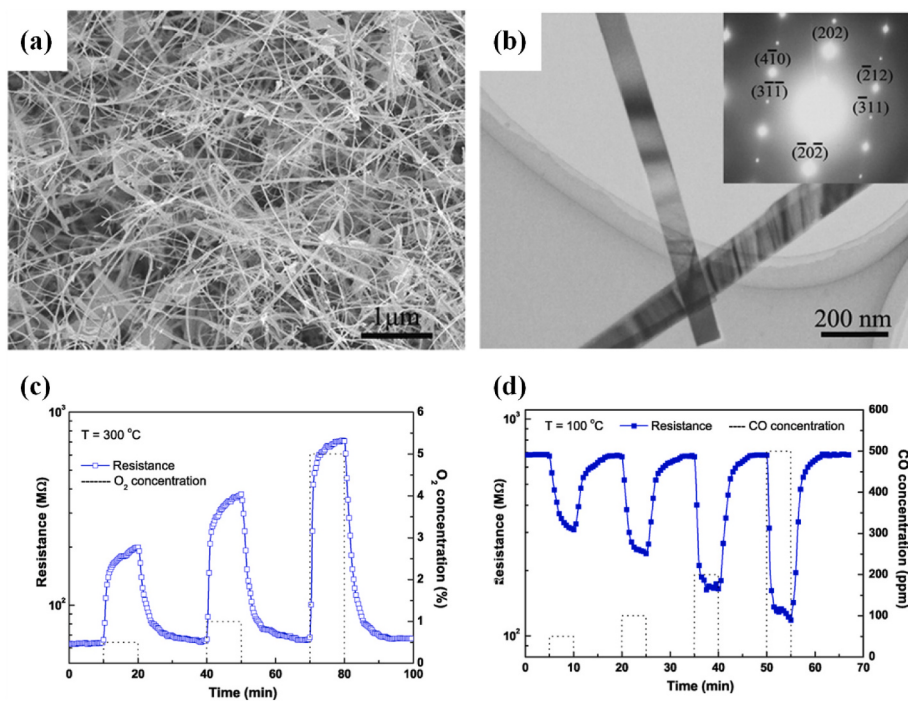


Fig. 8. (a) SEM image and (b) TEM image of Ga_2O_3 nanowires. Dynamic response of the Ga_2O_3 nanowire sensor to (c) O_2 gas pulse at $300\text{ }^\circ\text{C}$, and (d) CO gas pulse at $100\text{ }^\circ\text{C}$. Adapted with permission [44]. Copyright 2008, Elsevier.

Table 2

Summary of the performance parameters of Ga_2O_3 gas sensors exposed to O_2 [44,57–63].

Material	Operating temperature ($^\circ\text{C}$)	Response/Concentration	Normalized response	Response and recovery time ($\tau_{\text{res}}, \text{s}/\tau_{\text{rec}}, \text{s}$)	Limit of detection (ppm)	Detection range (ppm-ppm)	Ref.
β - Ga_2O_3 multiple nanowires	300	10.0/5 ppm	9.00	~150/600	10^{-2}	10^{-2} –5	[44]
β - Ga_2O_3 single crystal	850	0.70/ 10^{-1} ppm	0.70	12/20	10^{-1}	10^{-1} –100	[57]
Ce-doped Ga_2O_3 amorphous films	460	1.55/100 ppm	1.55	40/30	100	100–10000	[58]
Sb-doped Ga_2O_3 amorphous films	520	1.27/100 ppm	1.27	90/65	100	100–10000	[58]
W-doped Ga_2O_3 amorphous films	520	2.56/100 ppm	2.56	90/80	100	100–10000	[58]
Zn-doped Ga_2O_3 amorphous films	420	2.93/100 ppm	2.93	100/70	100	100–10000	[58]
Cr-doped β - Ga_2O_3 polycrystalline films	500	5.30/350 ppm	5.30	40/190	150	150–1600	[60]
	700	5.80/350 ppm	5.80	20/52	150	150–1600	[60]
Amorphous Ga_2O_3 films	900	~3.75/–	3.75	~60/60	–	–	[61]
Amorphous Ga_2O_3 films	1000	1.35/–	1.35	12/30	–	–	[62]
Polycrystalline β - Ga_2O_3 films	1000	1.80/–	2.70	14/–	–	–	[63]
	1000	1.40/–	2.50	27/–	–	–	[63]

(10^{-1} –1 ppm) due to the presence of high-density surface/interface states in nanowires. The LOD of Ga_2O_3 -based O_3 gas sensors is also as low as 10^{-2} ppm.

The high-density surface/interface states also decrease the desorption rate of adsorbed target gas and thereby increase the response time and response fluctuation of polycrystalline/amorphous or nanowires Ga_2O_3 gas sensors [69]. Furthermore, impurities and grain boundaries in Ga_2O_3 materials reduce the carrier mobility and thus increase the response time of Ga_2O_3 gas sensors [70]. Therefore, the response time of single-crystal Ga_2O_3 gas sensors (1–10 s) is shorter than that of metal-doped Ga_2O_3 thin film (10–100 s) or Ga_2O_3 nanowire (>60 s) or amorphous Ga_2O_3 (>100 s) gas sensors. A product ($S \times \tau^{-1}$) of response and response frequency is roughly estimated to be 0.1–1 for Ga_2O_3 -based O_2 gas sensors, which is limited by the basic gas sensing mechanism. The product can be improved at high operation temperature due to the enhancement of response and response speed by promoting the

absorption/desorption rate. Another problem in polycrystalline/amorphous or nanowires Ga_2O_3 gas sensors is response fluctuation, which reduces the stability of Ga_2O_3 gas sensors. The experimental results show that the response fluctuation of polycrystalline/amorphous or nanowire Ga_2O_3 gas sensors is higher than that of single-crystal Ga_2O_3 gas sensors [57,65,66]. Cleanse technologies are required and employed for the response recovery of Ga_2O_3 gas sensors to ensure its long-term stability. High-temperature anneal under appropriate ambient (e.g. air, N_2 , Ar , etc.) and high pressure have been employed for response recovery and long-term stability of the oxide gas sensors [55,71–73]. Recently, gas sensors fabricated from some materials and structures show fast response recovery and good long-term stability below $100\text{ }^\circ\text{C}$ for NO_x , H_2 , VOCs gas sensors, indicating the feasibility of fabricating cleanse-free oxide gas sensors of good long-term stability.

5.2. CO gas sensors

The CO acts as a reducing agent on the surface of oxides due to the reaction between CO and surface chemisorbed oxygen ions based on Equations (10)-(12) [74,75]. A low activation energy (0.1–0.6 eV) is observed for the reaction at operation temperature from 400 to 1000 °C [43]. Many CO gas sensors fabricated from oxide semiconductor materials, such as ZnO, SnO₂, In₂O₃, WO₃, CuO, Ti₂O and CeO₂ [76], usually possess an irreversible loss of performance at HT. In comparison, CO gas sensors fabricated from β-Ga₂O₃ are of long-term stability due to its high thermal stability. Hoefer et al. studied the CO sensing properties of commercially available SnO₂ and Ga₂O₃ gas sensors, among which the Ga₂O₃ gas sensor showed a stable response and the SnO₂ gas sensor showed obvious drift effects [29]. In 1998, Frank et al. studied the CO gas sensing properties of metal-doped polycrystalline β-Ga₂O₃ thick films [50]. A response of 4–5 was observed for the pure and Sn-doped Ga₂O₃-based CO gas sensors, and declined with the temperature. Vorobyeva et al. discovered that Sn dopants would be segregated as SnO₂ on the surface of Ga₂O₃ and increase the oxygen adsorption ability of Ga₂O₃ [77]. Therefore, the appropriate proper dopants and optimum operating temperature may enhance the performance of Ga₂O₃ gas sensors. Wu et al. further fabricated a CO gas sensor fabricated from Au-doped Ga₂O₃ film with impedance-metric yttria-stabilized zirconia (YSZ) [78]. A response time of 10 s, a recovery time of 10 s, and a response of ~1.66–800 ppm CO were observed at 550 °C. The response of Ga₂O₃ gas sensors to O₂ and CO is similar below 550 °C. The selectivity of CO gas sensors needs to be improved. The selectivity of CO gas sensors needs to be improved by modulating adsorption/desorption characteristics of O₂ and CO. During the CO sensing process, the produced carbon dioxide (CO₂) behaves as an oxidizing gas and has a negative interference on the detection of CO gas sensors [79,80]. Further study is needed to clarify the CO₂ adsorption on the surface of Ga₂O₃ [81,82].

The performance parameters of Ga₂O₃ thin films based CO gas sensors cannot satisfy most applications, instead researchers fabricate Ga₂O₃ nanostructures based CO gas sensors. As shown in Fig. 8, Liu et al. demonstrated a Ga₂O₃-multiple-nanowires CO gas sensor with a typical n-type response curve [44]. The CO response is 2–4 times higher than

the O₂ response at 100–200 °C. Kim et al. further reported CO gas sensing properties of Pt-functionalized β-Ga₂O₃ nanowires gas sensors [83]. A response of ~2.11–100 ppm CO is observed at 100 °C, which is higher than a response of ~1.07 for the pure β-Ga₂O₃ nanowires gas sensors. The enhancement of CO gas sensing is attributed to the increase of adsorbing and diffusing CO molecules on the β-Ga₂O₃ surface by Pt catalyst. The response time and recovery time of Pt-functionalized β-Ga₂O₃ nanowires gas sensors are 650 and 570 s, respectively, and larger than those of pure β-Ga₂O₃ nanowires gas sensors (440 and 300 s), as shown in Fig. 9.

The gas adsorption/desorption characteristics of Ga₂O₃-based gas sensors can be modulated by reduction of activation energy and diffusion barrier of target gases via decorating some noble metals on the Ga₂O₃ surface. This so-called spill-over effect has been applied to improve the performance of most gas sensors. Weng et al. studied Au decorated β-Ga₂O₃ nanowires gas sensors with a short response time of 5.85 s, a short recovery time of 10.13 s, and a response of ~1.08–2158 ppm CO at room temperature (RT) [84]. As a spill-over effect material, Au was a proper material to improve the response speed of Ga₂O₃-based CO gas sensors. The CO behavior on the oxides surface is strongly influenced by the reaction between CO and surface chemisorbed oxygen ions. The metal covering the oxide surface modulates the adsorption characteristics of the target gas and also the chemical reaction rate by concentration variations of surface chemisorbed oxygen ions. High metal coverage on the oxide surface significantly lowers the concentration of chemisorbed oxygen ions and thus suppresses the reduction reaction, and eventually CO becomes an oxidizing agent [85].

Park et al. fabricated a surface-nitridated Ga₂O₃ nanowires CO gas sensor with a maximum response of 3.63–200 ppm CO at 150 °C, which is 3.1 times larger than the response for pristine Ga₂O₃ nanowires gas sensors [86]. The response improvement is attributed to the increase of the depletion layer and a potential barrier by the Ga₂O₃/GaN interface [86,87]. Recently, Bui et al. reported a GaN/Ga₂O₃ core-shell nanowires based gas sensor with a high response to CO gas [88]. Lin et al. proposed a high-sensitivity gas sensor based on LSFO-nanoparticle-sensitize Ga₂O₃ nanorod arrays with a response of ~70, a response time of 200 s, and a recovery time of 500 s to 100 ppm CO at 500 °C, while the

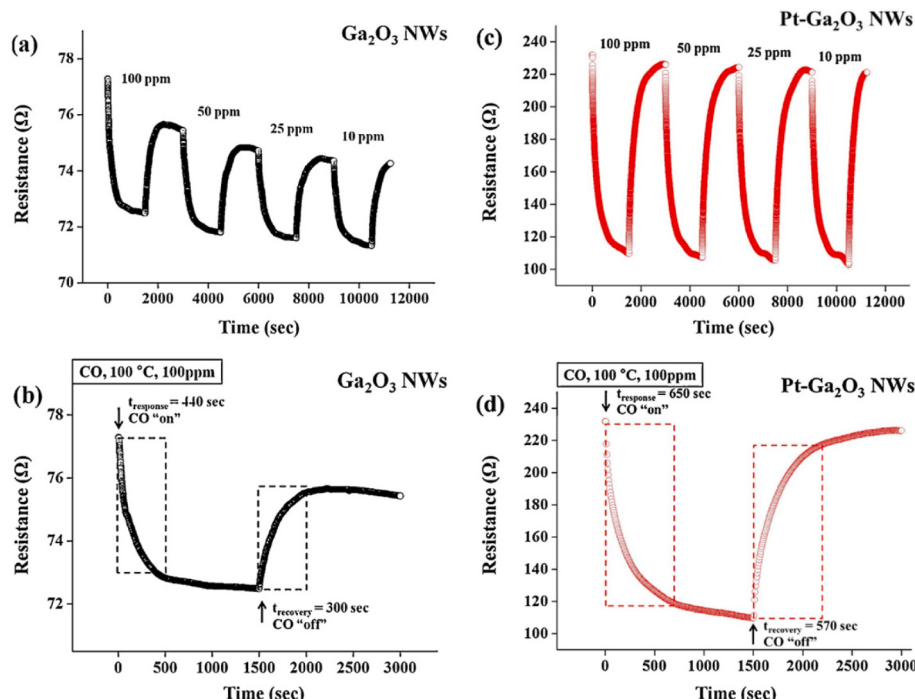


Fig. 9. Resistance curve of (a) pure Ga₂O₃ nanowires and (c) Pt-functionalized Ga₂O₃ nanowires gas sensors to 10, 25, 50, and 100 ppm CO at 100 °C and (b) enlarged curve of pure Ga₂O₃ and (d) enlarged curve of Pt-Ga₂O₃ nanowire. Adapted with permission [83]. Copyright 2012, Elsevier.

pristine Ga_2O_3 nanorod arrays gas sensor only showed a response of ~ 8 [89]. This sensing mechanism of metal-oxide-based core-shell nanostructures has been widely applied to improve the response, response speed and selectivity of oxide semiconductor gas sensors.

Tables 3 and 4 provide details regarding the performance parameters for the state-of-the-art Ga_2O_3 -based CO gas sensors [29,44,50,54,78,83, 84,86,89–92]. The normalized response of Ga_2O_3 polycrystalline thin film and nanowires gas sensors is 1–3 and $10\text{--}10^2$, respectively. The response time of Ga_2O_3 thin film and nanowire gas sensors is 10–100 s and 60–600 s, respectively. A product (S/τ) of ~ 0.1 is roughly obtained in Ga_2O_3 -based CO gas sensors. The LOD of Ga_2O_3 thin film and nanowires gas sensors is 10^2 ppm and 1–10 ppm, respectively. Interestingly, the operating temperature and activation energy of Ga_2O_3 -nanowires gas sensors are significantly lower than those of Ga_2O_3 -thin-film gas sensors, indicating the feasibility to fabricate high-performance low temperature (LT) Ga_2O_3 -based CO gas sensors. The Ga_2O_3 -based gas sensors exposed into CO and O_2 target gases reveal the similar long-term stability and response fluctuation. The same cleanse technologies are employed for the response recovery of Ga_2O_3 -based CO gas sensors and O_2 gas sensors [29,50,93]. A good selectivity of 3–7 is observed for Ga_2O_3 -based CO gas sensors at operation temperature below 300 °C, which is obtained by comparing the response of Ga_2O_3 -based gas sensors exposed to O_2 , CO, NO_x , VOCs, NH_3 , etc. [44,91].

5.3. NO_x gas sensors

The NO_x gas sensors fabricated from some oxide materials (SnO_2 , ZnO , WO_3 , In_2O_3 , Bi_2O_3 , Cu_2O , etc.) cannot operate at temperature above 400 °C [94]. The gas sensors fabricated from Ga_2O_3 have a wide operation temperature from RT to 1000 °C. Hoefer et al. reported that the surface depletion layer width of Ga_2O_3 -based gas sensors exposed into the NO_x target gas extended rapidly and quickly reached the Debye length below 750 °C [29]. The Ga_2O_3 -based NO_x gas sensors usually operate at LT and display a high LOD and a narrow concentration-detection window of the NO_x gas. Many methods have been employed to improve the sensitivity of Ga_2O_3 -based NO_x gas sensors at LT, such as applying spill-over effect, UV illumination and synthesis of nanostructure, core-shell nanostructure or nanocomposite heterostructure.

In 2010 Ma et al. reported a nitrogen dioxide (NO_2) gas sensor based on individual $\beta\text{-}\text{Ga}_2\text{O}_3$ nanobelts with a response time of 146 s and a low response to 100 ppm NO_2 [95]. Spill-over effect was recently applied to improve the response and selectivity of Ga_2O_3 -based NO_2 gas sensors. For instance, Zhang et al. decorated perovskite $\text{La}_{0.8}\text{Sr}_{0.2}\text{CoO}_3$ (LSCO) nanoparticles on $\beta\text{-}\text{Ga}_2\text{O}_3$ nanorod arrays for NO_2 gas sensing [96]. The

LSCO- Ga_2O_3 -based NO_2 gas sensors possessed a response of 32.6–200 ppm NO_2 at 800 °C and a response time of ~ 8 s (8 nm LSCO). The recovery time was about 1200 s and longer than that of pristine $\beta\text{-}\text{Ga}_2\text{O}_3$ gas sensor and most gas sensors. The long recovery time was attributed to a slow desorption kinetics of NO_2 and a slow decomposition rate on LSCO. The gas sensors fabricated from LSCO-decorated $\beta\text{-}\text{Ga}_2\text{O}_3$ nanorod arrays exhibited a high response and fast response speed. However, slow recovery was observed and indicated that LSCO may be not an appropriate spill-over effect material for Ga_2O_3 -based NO_x gas sensors.

An et al. applied both spill-over effect and UV illumination to enhance NO_2 sensing [53]. They fabricated a Pt-functionalized Ga_2O_3 nanorods gas sensor and a pristine- Ga_2O_3 nanorods gas sensor for comparisons. The response of pristine- Ga_2O_3 nanorods gas sensors was 2.98 under 5 ppm NO_2 ambient at RT. The response of Pt- Ga_2O_3 nanorods gas sensors to 5 ppm NO_2 was enhanced from 2.98 to 9.31 (1.75) at RT under 1.2 (0.35) mW/cm² UV illumination. Jin et al. reported $\text{Ga}_2\text{O}_3/\text{ZnO}$ core-shell nanorod gas sensors with a response of 327.78 to 100 ppm NO_2 at 300 °C, which is 692 times higher than the response of pristine Ga_2O_3 nanorod gas sensors and is 1790 times higher than the response of pristine ZnO nanorod gas sensors [97]. The recovery time decreased and the response time increased for the $\text{Ga}_2\text{O}_3/\text{ZnO}$ core-shell nanorod gas sensors, compared to the pristine ZnO or Ga_2O_3 nanorod gas sensors (Fig. 10). The increase of the response time is attributed to the relatively long time of electron transport from core to shell in the core-shell heterojunction. In 2020 Wang et al. studied NO_x gas sensor fabricated from $\text{Ga}_2\text{O}_3/\text{Al}_2\text{O}_3$ heterostructure nanocomposite (Fig. 11a–d) [48]. A response of 2.39 was obtained at RT for this NO_x gas sensor, higher than 1.10 for the pure- Ga_2O_3 -nanorods NO_x gas sensor (Fig. 11e–g). A low LOD of 500 ppb was observed for the $\text{Ga}_2\text{O}_3/\text{Al}_2\text{O}_3$ heterostructure nanocomposite gas sensor (Fig. 11e). The response improvement is attributed to the increase of O_2 and NO_x gas adsorption on the surface of porous $\text{Ga}_2\text{O}_3/\text{Al}_2\text{O}_3$ heterostructure nanocomposite.

At present, the Ga_2O_3 -based NO_x gas sensors are usually fabricated from nanowire or nanorod materials, and exhibit a high response (5–73) and a long response time (>60 s). Their critical performance parameters have been concluded in Table 5 [48,53,96–98]. Recently, the Ga_2O_3 -based polycrystalline and amorphous materials are also used to fabricate NO_x gas sensors [99–101]. The amorphous- Ga_2O_3 -based gas sensors display a high response of 25–72 (normalized response: 20), a long response time of 400–800 s, and a low activation energy of 0.52 eV, under 1–10 ppm NO_x ambient at RT or 200 °C. The polycrystalline- Ga_2O_3 -based gas sensors with a stack structure displayed a high response of ~ 5154 , and a long response time of $10^2\text{--}10^3$ s under 100 ppm NO_x ambient at 200 °C. A good selectivity is observed for this

Table 3
Summary of the performance parameters of Ga_2O_3 gas sensors exposed to CO [29,44,50,78,83,84,86,90–92].

Material	Operating temperature (°C)	Response/Concentration	Normalized response	Response and recovery time (τ_{res} , s/τ_{rec} , s)	Limit of detection (ppm)	Detection range (ppm-ppm)	Ref.
Polycrystalline Ga_2O_3 films	750	1.00/1500 ppm	2.00	–	100	100–1500	[29]
$\beta\text{-}\text{Ga}_2\text{O}_3$ multiple nanowires	100	3.15/200 ppm	4.12	$\sim 100/200$	50	50–500	[44]
Amorphous Ga_2O_3 films	755	2.25/400 ppm	2.50	–	400	–	[50]
Pt/YSZ/Au- Ga_2O_3 polycrystalline films	550	1.66/800 ppm	1.52	10/10	100	100–800	[78]
Pt-functionalized Ga_2O_3 nanowires	100	1.15/10 ppm	2.09	660/400	10	10–100	[83]
Ga_2O_3 nanowires	100	0.04/10 ppm	1.08	560/440	10	10–100	[83]
Au-decorated $\beta\text{-}\text{Ga}_2\text{O}_3$ nanowires	RT	0.05/100 ppm	–	21.14/21.34	100	100–2158	[84]
Surface-nitridated Ga_2O_3 nanowires	150	3.01/100 ppm	3.2	$\sim 100/300$	10	10–200	[86]
Ga_2O_3 nanowires	150	1.00/100 ppm	1.16	$\sim 100/300$	10	10–200	[86]
Mesoporous Ga_2O_3 nanoplate	RT	–	1.5	–	50	50	[90]
$\text{Ga}_2\text{O}_3/\text{In}_2\text{O}_3$ nanocomposite	350	18/300 ppm	–	23/18	–	–	[92]

Table 4Summary of the performance parameters of Ga_2O_3 nanorods gas sensors exposed to CO [54,89].

Material	Operating temperature (°C)	Response/Concentration	Normalized response	Response and recovery time ($\tau_{\text{res}}, \text{s}/\tau_{\text{rec}}, \text{s}$)	Limit of detection (ppm)	Detection range (ppm-ppm)	Ref.
Ga_2O_3 nanorods ^a	500	6.45/100 ppm	5.00	699/690	–	–	[54]
Ga_2O_3 nanorods ^b	500	8.39/100 ppm	8.00	622/490	–	–	[54]
LSFO/ Ga_2O_3 nanorods ^a	500	64.63/100 ppm	45.00	700/200	–	–	[54]
LSFO/ Ga_2O_3 nanorods ^b	500	77.56/100 ppm	52.50	500/270	–	–	[54]
1 nm Pt– Ga_2O_3 nanorods ^a	500	68.50/100 ppm	45.00	651/122	–	–	[54]
1 nm Pt– Ga_2O_3 nanorods ^b	500	189.9/100 ppm	70.00	400/200	–	–	[54]
5 nm Pt– Ga_2O_3 nanorods ^a	500	300.1/100 ppm	–	222/393	–	–	[54]
5 nm Pt– Ga_2O_3 nanorods ^b	500	289.0/100 ppm	–	290/440	–	–	[54]
Ga_2O_3 nanorods	500	8/100 ppm	2.5	100/500	20	20–100	[89]
10 nm LSFO/ Ga_2O_3 nanorods	500	70/100 ppm	37.5	200/500	20	20–100	[89]
Pt– Ga_2O_3 nanorods	500	95/100 ppm	46	620/500	20	20–100	[89]
$\beta\text{-}\text{Ga}_2\text{O}_3$ nanorods	100	1.00/5 ppm	1.94	30/37	1	1–5	[91]
$\beta\text{-}\text{Ga}_2\text{O}_3$ rectangular nanorods	100	0.65/1 ppm	1.03	59/60	1	1–5	[91]

^a Without UV illumination.^b With UV illumination, LSFO: $\text{La}_{0.8}\text{Sr}_{0.2}\text{FeO}_3$.

Ga_2O_3 -based NO_x gas sensor at 200 °C, and a poor selectivity exists in other Ga_2O_3 -based NO_x gas sensors. In general, a high NO_x gas sensing with a long response time is observed in the Ga_2O_3 -based gas sensors. The response fluctuation of NO_x gas sensing is higher than that of CO and O₂ gas sensing for Ga_2O_3 -based gas sensors [94–96]. The response recovery is not significantly improved at high operation temperature, indicating that the current cleanse technologies require improvement to ensure the long-term stability of Ga_2O_3 -based NO_x gas sensors.

The LOD of Ga_2O_3 -based NO_x gas sensors is 1–10 ppm at temperature from RT to 350 °C and remarkably changes to 200–10³ ppm above 350 °C. This LOD does not satisfy the requirements of health and safety guidelines (lower than 3 ppm) and the detection of NO breathed out from asthma patients (lower than 100 ppb) [102–105]. The high LOD for NO_x gas detection is also present in other oxides-based gas sensors and attributed to the complex nitrite-correlated reactions [106–109]. Recently, UV-visible illumination, van der Waals heterostructures with graphene, perovskite and transition metal dichalcogenides (TMDs) are proposed to improve the gas sensing and long-term stability of oxides-based NO_x gas sensors [41,96,110–117]. For instance, the gas sensors fabricated from the TMDs/oxides heterostructures have a response of 35, a response time of 2 s, and a recovery time of 30 s under 50 ppm NO_x at RT, with a low LOD of 0.01 ppm, indicating an improvement of the NO_x gas sensing and response recovery [41,118]. The improvement of the NO_x gas sensing is attributed to the increase of adsorption capacity by high-density interlayer carriers and excitons in van der Waals heterostructures. Further study is required to clarify NO_x gas sensing mechanisms and develop novel methods to improve NO_x gas sensing of Ga_2O_3 -based NO_x gas sensors.

5.4. H_2 gas sensors

Early H_2 gas sensors were mostly fabricated from Si, SiC, and GaN materials. The Si-based gas sensors cannot operate at HT and SiC and GaN-based gas sensors suffer from a limit of response [119–122]. Recently, $\beta\text{-}\text{Ga}_2\text{O}_3$ -based H_2 gas sensors were fabricated with high performance and good thermal stability. An O–H configuration is formed on the $\beta\text{-}\text{Ga}_2\text{O}_3$ surface with negative enthalpies of H_2 adsorption, which introduces shallow donors and high-density surface states and thus changes the surface Fermi level [123–127], as shown in Fig. 12a. The donor-like behavior of O–H configuration is similar to that of CO

adsorption on the oxide surface, and indicates that H_2 gas acts as a reducing agent for the Ga_2O_3 gas sensors [128,129]. This O–H configuration induces a small activation energy of 0.1–0.3 eV (~1.99 kJ/mol) for H_2 sensing and thus is responsible for the high response and selectivity [123,126,130], indicating the feasibility to fabricate high-performance Ga_2O_3 -based H_2 gas sensors from RT to HT.

In 1993 Fleischer et al. reported H_2 gas sensing of polycrystalline Ga_2O_3 film at high operation temperature (>500 °C) for the first time [128,129]. A high response of >100 was observed for Ga_2O_3 -based H_2 gas sensor at an operation temperature of 550 °C, indicating a considerable potential of Ga_2O_3 gas sensor in applications of H_2 gas sensing. Meanwhile, amorphous oxides gas sensors were also fabricated and exhibited a high response of 18 [131]. In 2009 Cuong et al. exhibited LT H_2 gas sensors fabricated from vapor-liquid-solid-grown $\beta\text{-}\text{Ga}_2\text{O}_3$ nanowires. This H_2 gas sensor had a response of 6.3 and a response time of 43 s–200 ppm H_2 [132]. Yan et al. fabricated Pt/ $\beta\text{-}\text{Ga}_2\text{O}_3$ /GaN metal/insulator/semiconductor type H_2 gas sensors [130]. The response of Pt/4 nm $\beta\text{-}\text{Ga}_2\text{O}_3$ /GaN type gas sensors is 38.5–100 ppm H_2 at RT and much higher than that of Pt/GaN MS-type gas sensors (response: 1.5). The corresponding response time of Pt/ $\beta\text{-}\text{Ga}_2\text{O}_3$ /GaN type gas sensors is 11.8 s and much shorter than that of MS-type gas sensors (37 s), as shown in Fig. 12b. The influence of $\beta\text{-}\text{Ga}_2\text{O}_3$ thickness (4, 15, 60 nm) on improving gas sensing was investigated and attributed to the increase of oxygen ions density at surface with $\beta\text{-}\text{Ga}_2\text{O}_3$ thickness. Jang et al. proposed a Schottky-diodes H_2 gas sensor based on (–201) and (010) Ga_2O_3 wafer, with a response of 7.86×10^5 (1.58×10^5) at 0.8 (1.5) V to 500 ppm H_2 at RT [133]. A short response time of less than 2 s and a low LOD of 0.01 ppm is obtained by measuring current variations of single-crystal (010) Ga_2O_3 diode sensors exposed to different H_2 concentrations. The current variations of sensors under H_2 , N_2 , CO, CO_2 , O_2 , CH_4 , NO_2 and NH_3 indicated that single-crystal (010) Ga_2O_3 Schottky-diodes gas sensors had a good selectivity to H_2 (Fig. 12c). Abdullah et al. reported a H_2 gas sensor fabricated from SnO_2 -coated $\beta\text{-}\text{Ga}_2\text{O}_3$ nanostructures with a response of 7074.5 to 1000 ppm H_2 at 200 °C [45]. The response time and recovery time were as high as 100–300 s. Almaev et al. reported a Sn-doped single-crystal Ga_2O_3 -based H_2 gas sensors with a response of 80–1000 ppm H_2 at 350 °C [134]. The devices show a short response time of 10 s, a long-term stability of 40 days, and a LOD of 50 ppm.

Although O–H configuration enhances the sensitivity and selectivity of Ga_2O_3 -based H_2 gas sensors, a strong response fluctuation and a poor

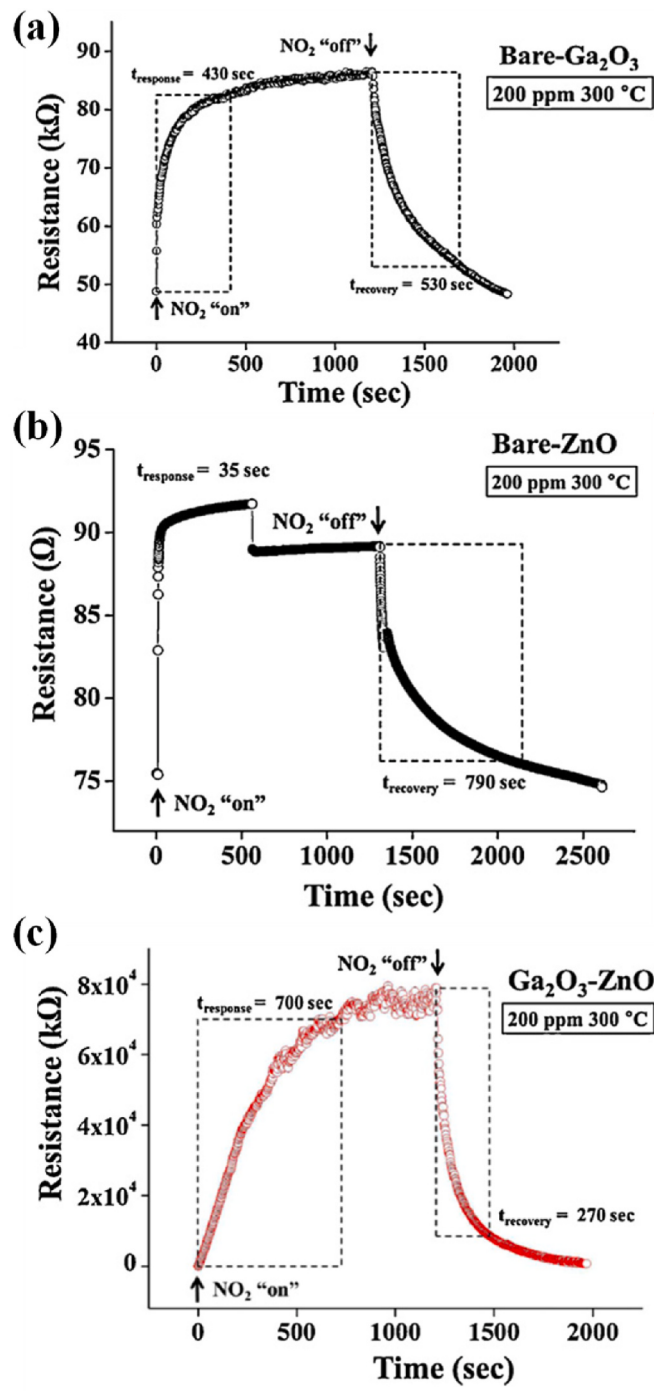


Fig. 10. Resistance curve of (a) bare-Ga₂O₃ nanorod, (b) bare-ZnO nanorod, and (c) Ga₂O₃-ZnO core-shell nanorod to 200 ppm NO₂ at 300 °C. Adapted with permission [97]. Copyright 2012, Elsevier.

recovery are also induced by O-H configuration and another large-negative-enthalpies structures of H and O-vacancies/defects [123, 135]. The hydrogen sensing performance of β -Ga₂O₃ is also influenced by some special situations in a real environment, such as temperature fluctuation, different oxygen concentrations, gas flow rate change, etc. Recently, Nakagomi et al. demonstrated self-compensated H₂ gas sensors, which is achieved by the cascade of β -Ga₂O₃ resistance type and field-effect type H₂ gas sensors [133,136]. The self-compensated H₂ gas sensors exhibit perfect stability for sensing performance under temperature fluctuating over 100 °C (Fig. 13a). It indicates that appropriate device structure may improve the sensing performance of β -Ga₂O₃ gas

sensors.

Table 6 shows details regarding the performance parameters of the state-of-the-art Ga₂O₃-based H₂ gas sensors [130,132,133,136]. The normalized response of various Ga₂O₃ materials is as high as 30 or higher, and the LOD can reach 0.01 ppm. The response time of single-crystal Ga₂O₃ and Ga₂O₃ nanowire gas sensors is 10–40 s and shorter than that of polycrystalline and amorphous Ga₂O₃ gas sensors (>60 s). The response fluctuation of single-crystal Ga₂O₃ gas sensors is less than that of polycrystalline or amorphous Ga₂O₃ gas sensors [134, 137]. Good selectivity can be obtained at LT for the Ga₂O₃-based H₂ gas sensors [133,134]. Recently, a novel high-performance H₂ gas sensor was fabricated from the mesoporous group-III oxides [138]. This mesoporous H₂ gas sensor possessed a high response of 18–500 ppm H₂, an ultra-short response time and recovery time (1.7 s and 1.5 s), a low LOD of 10 ppb, and a low response fluctuation as well as good long-term stability of 280 days (Fig. 13b). The single-crystal and mesoporous group-III oxides show great potentials for gas sensing of H₂ target gas due to its special O-H configuration.

5.5. Other gas sensors

Currently, it is difficult to fabricate a Ga₂O₃-based VOCs gas sensor with a good selectivity. Fleischer et al. and Frank et al. reported that pristine Ga₂O₃ films gas sensors respond to many kinds of VOCs, such as methane, propane, isobutane [49,50]. Wu et al. reported an isopropyl alcohol (IPA) sensor based on β -Ga₂O₃ nanowires with a response of 1.49–400 ppm IPA at 300 °C and a response time of less than 5 s [139]. Most researchers studied the sensing properties of Ga₂O₃ heterostructures to further enhance the selectivity. Bagheri et al. studied the sensing performance of Ga₂O₃/In₂O₃ nanocomposite with different Ga₂O₃ content (wt%) [92]. A HT calcination is applied to modify the surface structure of nanocomposite. Good VOCs gas sensing is observed in the 10 wt% Ga₂O₃/90 wt% In₂O₃ nanocomposite (IG10), the 25 wt% Ga₂O₃/75 wt% In₂O₃ nanocomposite (IG25), the 65 wt% Ga₂O₃/35 wt% In₂O₃ nanocomposite (IG65), and the 75 wt% Ga₂O₃/25 wt% In₂O₃ nanocomposite (IG75). IG10, IG25, and IG65 gas sensors calcined at 500 °C had a maximum response of 69.1–300 ppm ethanol at 300 °C, 26.5–300 ppm CO at 300 °C, and 38.5 to 1% CH₄ at 400 °C, respectively. IG75 gas sensors calcined at 850 °C had a better selectivity to 300 ppm CO at 350 °C, and exhibited a better selectivity to 1% CH₄ at 650 °C. Dyndal et al. reported the acetone detection capability of CuO/Ga₂O₃ thin films with different gallium oxide content (wt%) [47]. A maximum response of 1.3 was observed under 1.25 ppm acetone at 300 °C for CuO/(4 wt%)Ga₂O₃ gas sensors with a response time 185 s, a recovery time of 525 s, and a LOD of 0.1 ppm. A relatively low humidity influence on the detection of VOCs for Ga₂O₃-based gas sensors was observed. Song et al. investigated SnO₂/MO_x (M = Zn, Ga and W) heterostructure nanomaterials for fabricating highly selective gas sensors [140]. The gas sensors fabricated from SnO₂/Ga₂O₃ nanotubes with Brunauer-Emmett-Teller (BET) specific area of 583.8 m²/g exhibited a high response of 32.4–100 ppm ethanol at 300 °C, a short response time of 2 s, and a good selectivity for ethanol (Fig. 14a). Wei et al. studied Ga₂O₃/WO₃ heterostructures for ethanol detection [141]. The Ga₂O₃/WO₃ gas sensors had a response of 14–100 ppm ethanol at 275 °C, a short response time of 5 s, a recovery time of 3 s, and a LOD of 1 ppm. Both SnO₂/Ga₂O₃ and Ga₂O₃/WO₃ gas sensors show a considerable response to acetone. In addition, the LOD of acetone sensing would decrease to 0.1 ppm in the amorphous Ga₂O₃ transistor-type gas sensors at RT, and a long response time of >60 s was also observed [99]. Recently, Krawczyk et al. discovered a good VOCs sensing in β -Ga₂O₃ nanowires [142]. A maximum response of 75.1 (27.5) to 100 ppm ethanol was observed at 760 (690) °C. However, the selectivity of these β -Ga₂O₃ nanowires gas sensors was poor.

Ammonia is a toxic and strong reducing gas, and the Occupational Safety and Health Administration established the maximum recommended exposure level of NH₃ to be 25 ppm. Thus, NH₃ gas sensors

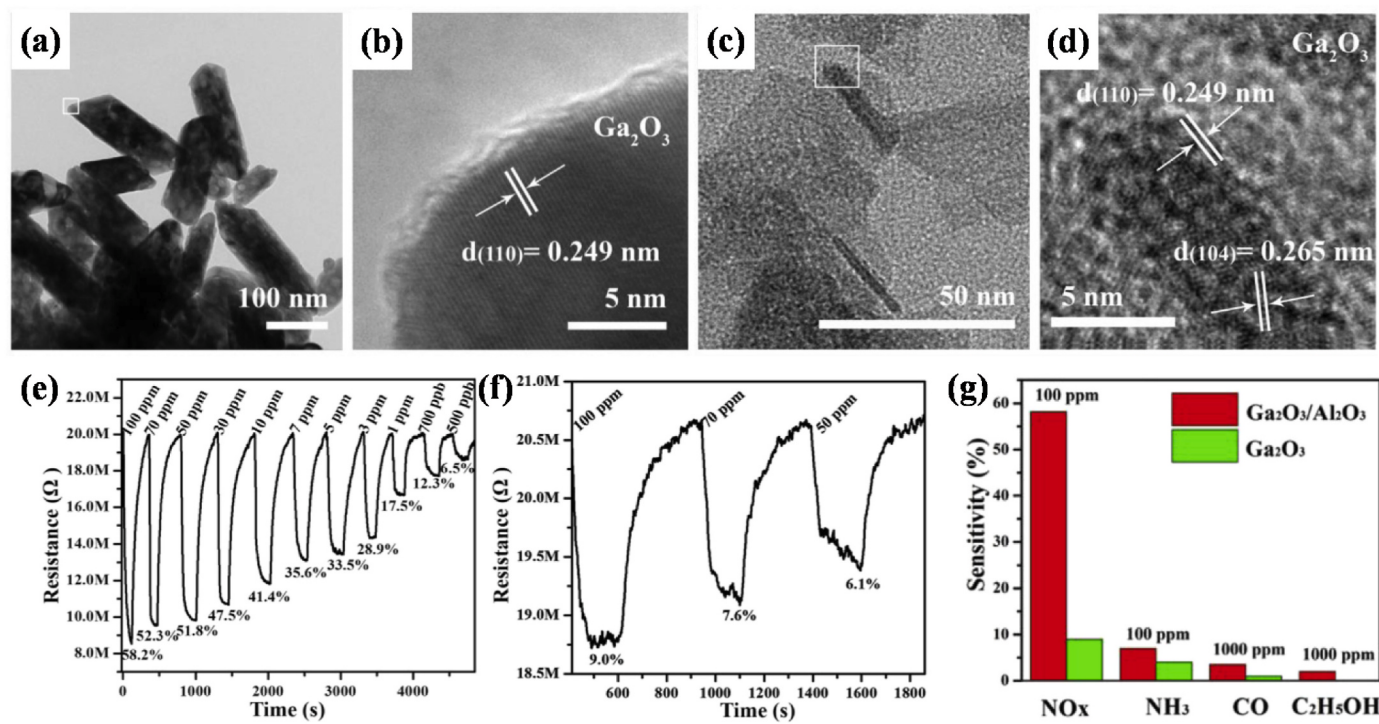


Fig. 11. TEM images of (a) pure Ga₂O₃ and (c) Ga₂O₃/Al₂O₃ composite, together with their respective local HRTEM images in (b) and (d). Gas sensing sensitivity to NO_x of (e) Ga₂O₃/Al₂O₃ composite and (f) pure Ga₂O₃. (g) Response of the Ga₂O₃/Al₂O₃ composite sensor to various gases at RT. Adapted with permission [48]. Copyright 2020, Elsevier.

Table 5

Summary of the performance parameters of Ga₂O₃ gas sensors exposed to NO₂ [48,53,96–98].

Material	Operating temperature (°C)	Response/Concentration	Normalized response	Response and recovery time ($\tau_{\text{res}}, \text{s}/\tau_{\text{rec}}, \text{s}$)	Limit of detection (ppm)	Detection range (ppm-ppm)	Ref.
Ga ₂ O ₃ /Al ₂ O ₃ nanocomposite	RT	0.07/0.5 ppm	1.07	>100	0.5	0.5–100	[48]
Ga ₂ O ₃ nanorods ^b	RT	2.98/5 ppm	2.2	100/230	1	1–5	[53]
Pt–Ga ₂ O ₃ nanorods ^a	RT	–/5 ppm	1.8	200/300	1	1–5	[53]
Pt–Ga ₂ O ₃ nanorods ^b	RT	9.31/5 ppm	9.43	110/230	1	1–5	[53]
β-Ga ₂ O ₃ nanorods	800	5.12/200 ppm	7.31	23/900	200	200–500	[96]
3 nm LSCO/β-Ga ₂ O ₃ nanorods	800	25.70/200 ppm	19.00	7.5/1150	200	200–500	[96]
8 nm LSCO/β-Ga ₂ O ₃ nanorods	800	32.60/200 ppm	12.00	9/1150	200	200–500	[96]
β-Ga ₂ O ₃ nanorods	300	0.77/200 ppm	1.76	430/530	10	10–200	[97]
β-Ga ₂ O ₃ /ZnO nanorods	300	72.47/10 ppm	–	840/400	10	10–200	[97]
Pd-doped Ga ₂ O ₃ nanowires	RT	0.41/100 ppm	1.46	200/70	10	10–100	[98]

^a Without UV illumination.

^b With UV illumination, LSCO: La_{0.8}Sr_{0.2}CoO₃.

should possess a LOD less than 25 ppm to ensure safety. Recently, the β-Ga₂O₃ materials have been applied to fabricate the NH₃ gas sensors. Pandeeswari et al. fabricated a β-Ga₂O₃ thin film NH₃ gas sensor with a response of 1.19 to 0.5 ppm NH₃ at RT, a response time of 40 s, a recovery time of 18 s, a LOD of 0.5 ppm, and a low response saturation of 50 ppm [46]. Pilliadugula et al. fabricated a hierarchical-structure β-Ga₂O₃ cluster gas sensors with good NH₃ sensing [143,144]. Undoped β-Ga₂O₃ cluster gas sensors showed a response of ~2.85–200 ppm NH₃ at RT (Fig. 14b). Sn-doped β-Ga₂O₃ cluster gas sensors exhibited a response of ~3.75–200 ppm NH₃ at RT, which is fabricated from a special β-Ga₂O₃ cluster with 2 mol% Sn-doped concentration, 12.49 m²/g BET, and 11.64 nm pore size (Fig. 14 c). The response of β-Ga₂O₃ cluster gas sensors increased with BET surface area induced by Sn doping. Recently, the amorphous Ga₂O₃-based NH₃ gas sensors has been demonstrated and had a similar response with β-Ga₂O₃ thin film NH₃ gas

sensors. A LOD of 0.1 ppm, and a long response time of >60 s was observed at RT [99]. Pt nanoparticles coated amorphous Ga₂O₃ gas sensors show a response of 1467, a response time of 31 s, and a recovery time of 15 s at 250 °C, respectively [145].

Currently, the studies on Ga₂O₃-based VOCs and NH₃ gas sensors are rare, and most studies focus on nanostructure and polycrystalline Ga₂O₃ gas sensors. Table 6 shows details regarding the performance parameters of the state-of-the-art Ga₂O₃-based gas sensors exposed to NH₃, ethanol, IPA, and acetone [46,47,92,139–141,143]. The gas sensing of VOCs and NH₃ is similar with the gas sensing of H₂ in Ga₂O₃ materials due to its special O–H configuration. The normalized response of Ga₂O₃-based VOCs and NH₃ gas sensors is 10–30. For the VOCs detection, the response time of Ga₂O₃ nanostructure gas sensors is ~10 s and shorter than that of polycrystalline and amorphous Ga₂O₃ gas sensors (>60 s). The response fluctuation of the Ga₂O₃-based VOCs gas sensors is similar

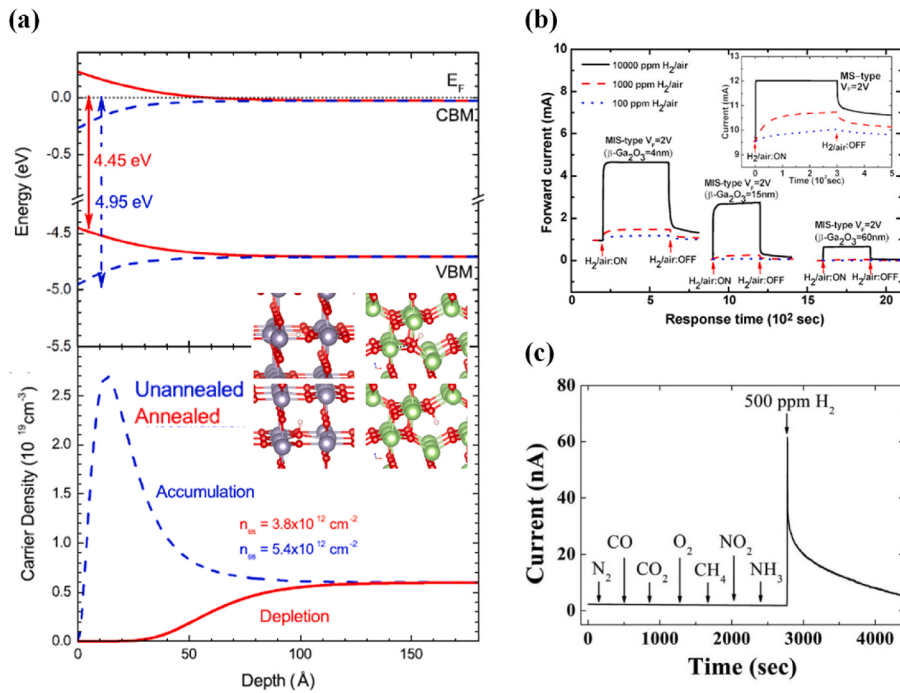


Fig. 12. (a) The band bending and carrier density profiles in the electron accumulation (blue) and depletion (red) surface layers for $\beta\text{-Ga}_2\text{O}_3$ obtained by Poisson-Thomas-Fermi-approximation calculations. The inset is the atomic structure schematic of O–H configurations. (b) Transient response curves of the Ga₂O₃-based H₂ gas sensors. (c) Transient response curves of Schottky-diodes H₂ gas sensors on the (010) Ga₂O₃ single crystal exposed to various gas species, including 0.1% CO, 4% CH₄, 10% CO₂, 0.05% NO₂, 2 ppm NH₃, and 500 ppm H₂ in N₂. (a) Adapted with permission [123]. Copyright 2019, American Institute of Physics. (b) Adapted with permission [130]. Copyright 2009, Elsevier. (c) Adapted with permission [133]. Copyright 2018, IOP science. (For interpretation of the references to colour in this figure legend, the reader is referred to the Web version of this article.)

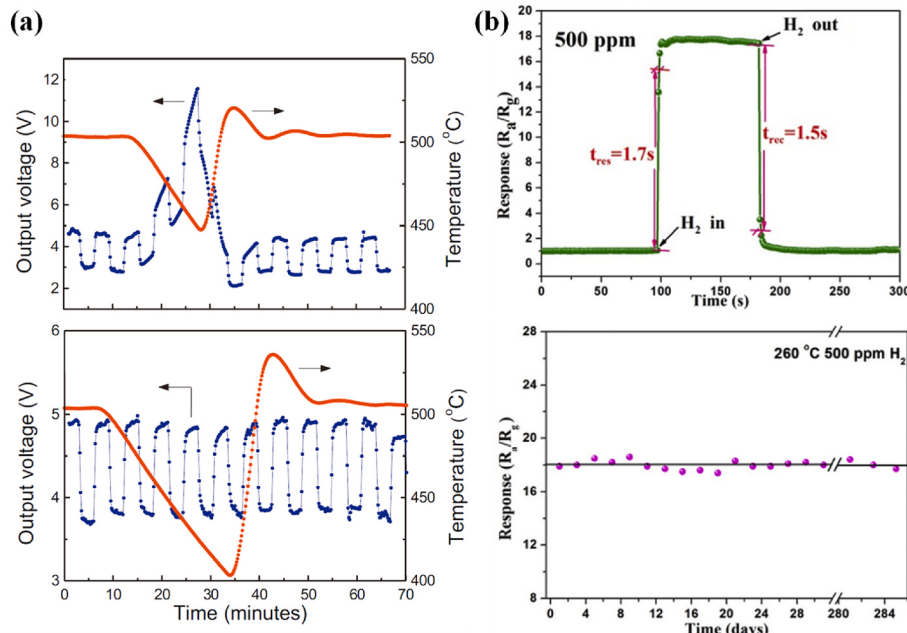


Fig. 13. (a) Output voltage curve under temperature fluctuation of single device (resistance type or field-effect type) and in-series connected device. (b) The transient response curve and stability of mesoporous H₂ gas sensors to 500 ppm H₂ at 260 °C. (a) Adapted with permission [136]. Copyright 2013, Elsevier. (b) Adapted with permission [138]. Copyright 2018, Elsevier.

with that of Ga₂O₃-based H₂ gas sensors. For the NH₃ detection, the response time of Ga₂O₃ nanostructure gas sensors slightly increases to 30–40 s, which is attributed to the complex N–H–O-correlated reactions. The LOD can reach 0.1 ppm and satisfies the standard of Occupational Safety and Health Administration. The Ga₂O₃-nanostructure or polycrystalline-Ga₂O₃ NH₃ gas sensors show a long-term stability, whereas amorphous Ga₂O₃ NH₃ gas sensors show a significant response fluctuation [46,143–147]. Recently, some studies demonstrate a strong H₂ sensing of amorphous oxides hollow-rounded cubes and chlorine (Cl₂) sensing of ferrite oxides [148,149]. Accordingly, Ga₂O₃-based gas

sensors have a large potential in the detection of VOCs, NH₃, H₂S, Cl₂, and so on.

The design and fabrication of Ga₂O₃-based humidity gas sensors have also attracted intense research interest due to its high humidity stability and ultrafast H–O absorption. In 2012 Liu et al. demonstrated a RT flexible Ga₂O₃-based humidity sensor on strained $\beta\text{-Ga}_2\text{O}_3/\text{SnO}_2$ core-shell microribbons with a response time of 28 s, a recovery time of 7 s, and a high response of 41 under 75% RH [150,151], as shown in Fig. 15a. The response enhancement under mechanical strain was attributed to the increase of humidity adsorption capacity with the

Table 6

Comparisons of the performance parameters of Ga_2O_3 gas sensors exposed to various target gases such as H_2 , NH_3 , Ethanol, IPA, Acetone [46,47,92,130,132,133,136, 140–142,144].

Material	Operating temperature ($^{\circ}\text{C}$)	Response/Concentration	Normalized response	Response and recovery time (τ_{res} , s/ τ_{rec} , s)	Limit of detection (ppm)	Detection range (ppm-ppm)	Ref.
Cr-doped Ga_2O_3 polycrystalline films	500	44.00/– H_2	–	–	–	–	[60]
4 nm β - $\text{Ga}_2\text{O}_3/\text{GaN}$	RT	37.50/100 ppm H_2	10	11.8/–	100	100–10000	[130]
60 nm β - $\text{Ga}_2\text{O}_3/\text{GaN}$	RT	2362/ 10^4 ppm H_2	10^3	1.6/–	100	100–10000	[130]
Ga_2O_3 nanowires	300	34.0/ 10^3 ppm H_2	50	48/>200	20	20–1000	[132]
β - Ga_2O_3 single crystal	RT	105/ 500 ppm H_2	$10\text{--}10^5$	2/>500	10–2	10^{-2} –40000	[133]
Polycrystalline β - Ga_2O_3 films	RT	332.5/ 50 ppm NH_3	18.8	40/420	0.5	0.5–100	[46]
Ga_2O_3 nanorods	RT	1.80/200 ppm NH_3	–	–	20	20–200	[143]
$\text{Ga}_2\text{O}_3/\text{In}_2\text{O}_3$ nanocomposite	300	69.0/300 ppm ethanol	60	13/42	–	–	[92]
$\text{SnO}_2/\text{Ga}_2\text{O}_3$ nanotubes	300	32.0/100 ppm ethanol	20	2/37	10	10–100	[140]
Amorphous Ga_2O_3 films	275	~1.60/100 ppm ethanol	1.3	5/9	~50	50–600	[141]
Amorphous $\text{Ga}_2\text{O}_3/\text{WO}_3$ films	275	14.0/100 ppm ethanol	13	5/3	1	1–600	[141]
β - Ga_2O_3 nanowires	300	0.23/400 ppm IPA	0.2	5/60	100	100–400	[139]
Polycrystalline $\text{CuO}/\text{Ga}_2\text{O}_3$ films	300	1.35/1.25 ppm acetone	1.41	394/563	0.1	0.1–1.25	[47]

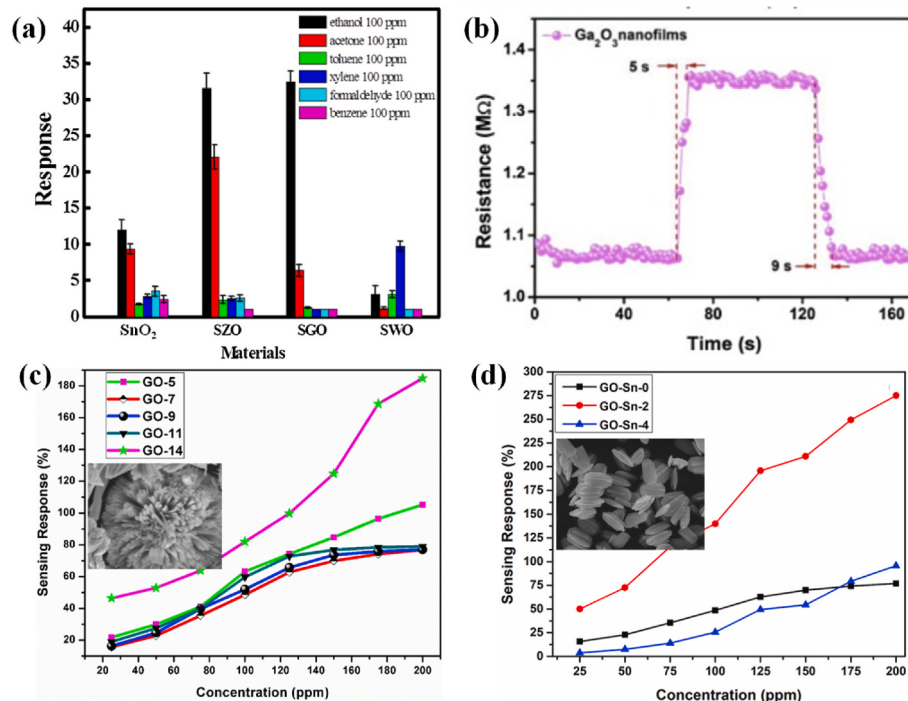


Fig. 14. (a) Response of gas sensors fabricated from SnO_2 , SnO_2/ZnO nanotubes (SZO), $\text{SnO}_2/\text{Ga}_2\text{O}_3$ nanotubes (SGO), and SnO_2/WO_3 nanofibers (SWO), exposed to 100 ppm ethanol, acetone, toluene, xylene, formaldehyde and benzene at 300 °C. (b) Transient response of amorphous $\text{Ga}_2\text{O}_3/\text{WO}_3$ gas sensors exposed to 100 ppm ethanol at 275 °C. (c) Response of undoped β - Ga_2O_3 cluster gas sensors exposed to different concentration NH_3 at RT. Inset is the SEM image of hierarchical-morphology β - Ga_2O_3 cluster (GO-14). (d) Response of Sn-doped β - Ga_2O_3 cluster exposed to different concentration NH_3 at RT. Inset is the SEM image of 2 mol% Sn-doped β - Ga_2O_3 cluster (GO-Sn-2). (a) Adapted with permission [140]. Copyright 2019, Elsevier. (b) Adapted with permission [141]. Copyright 2019, Elsevier. (c) Adapted with permission [143]. Copyright 2020, Elsevier. (d) Adapted with permission [144]. Copyright 2021, Elsevier.

stress-induced effective surface area of the shell SnO_2 sensitive material. In 2015 Juan et al. proposed a self-powered amorphous- Ga_2O_3 -based humidity sensor, obtained by the cascade of the amorphous- Ga_2O_3 sensor and the amorphous- WO_3 sensor [152]. This humidity sensor showed a response time of 43 s, a recovery time of 15 s, and a response of ~0.3 at 80% RH. Wang et al. discovered a humidity sensor fabricated from Na/K-codoped Ga_2O_3 nanorods with a high response of $10\text{--}10^4$, a short response time of 6 s, and a short recovery time of 21 s in the range of 11–95% RH [153], as shown in Fig. 15b. However, the device exhibited an obvious response fluctuation after 25 days. In 2018 Nakata et al. reported a wearable pH humidity sensor on amorphous Ga_2O_3 -based materials with a response less than 0.1, and a response time on the order of ms [154], as shown in Fig. 15c. In addition, the humidity sensor fabricated from controllably-constructed Ho_2O_3 nanomaterials had a

high response of $\sim 10^3$, and a short response time of 0.3 s, and a recovery time of 6 s in the range of 11–95% RH [42]. These sesquioxides (Ga_2O_3 , Ho_2O_3 , etc.) display a similar good humidity sensing with a high response ($10^3\text{--}10^4$) and an ultra-short response time (0.1–10 s), indicating an enormous potential for humidity detection.

6. Conclusions and future prospects

This article comprehensively presents recent advances in gas sensing mechanisms, performance parameters, influence factors, and applications of Ga_2O_3 -based gas sensors. The impacts of influence factors, doping, material structure and device structure on the performance of gas sensors are discussed in detail. The Ga_2O_3 -based gas sensors show high response to reducing and oxidizing gases. The Ga_2O_3 -based O_2 and

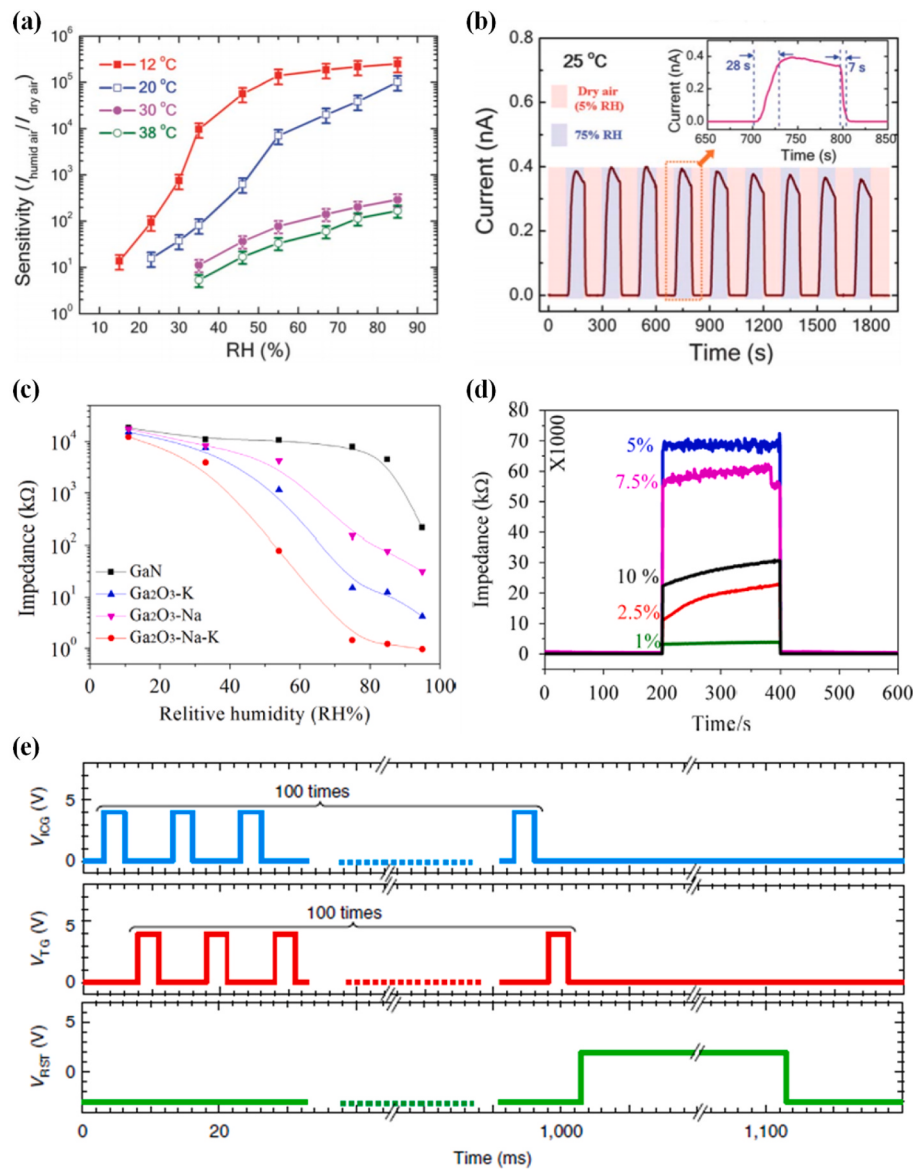


Fig. 15. (a) The sensitivity versus RH at different operation temperatures and (b) the corresponding transient response for the humidity sensor on strained β -Ga₂O₃/SnO₂ core-shell microribbons. (c) The impedance versus RH and (d) the impedance versus times for the humidity sensor fabricated from Na/K-codoped Ga₂O₃ nanorods. (e) The pH monitoring curve of the amorphous Ga₂O₃-based humidity sensor. (a) and (b) Adapted with permission [151]. Copyright 2012, The Royal Society of Chemistry. (c) and (d) Adapted with permission [153]. Copyright 2015, Elsevier. (e) Adapted with permission [154]. Copyright 2018, Springer Nature.

CO gas sensors of long-term stability have been fabricated and commercialized. Good selectivity has been demonstrated for Ga₂O₃-based O₂, CO, and H₂ gas sensors. On the way to the commercialization of Ga₂O₃-based gas sensors, there are at least but not limited to the following unsolved issues:

- (a) The achievement of Ga₂O₃ materials with good p-type conductivity and stability is a big challenge. Fundamental issues are the large formation energy, thermodynamics transition level (activation energy) and ionization energy of acceptor impurities. Other issues include hole self-trapping and self-compensation effects of cation and oxygen vacancies, and low hole mobility due to the flat valence band mainly contributed from the highly localized O2p orbitals. The p-type Ga₂O₃ gas sensors are seldom reported due to the lack of p-type Ga₂O₃ materials. The gas sensing properties of p-type Ga₂O₃ have not been investigated.
- (b) For Ga₂O₃-based NO_x gas sensors, its LOD does not satisfy requirements of health and safety guidelines and the detection of NO breathed out from asthma patients.
- (c) For Ga₂O₃-based H₂ gas sensors, the polycrystalline, amorphous and nanostructure Ga₂O₃ gas sensors suffer from a strong

response fluctuation and a poor response recovery, due to the existence of two large-negative-enthalpies H-correlated structures, i.e. O–H configuration as well as H and O-vacancies/defects.

- (d) The Ga₂O₃-based H₂, NO_x, NH₃, CO₂, and VOCs gas sensors have not been commercialized yet. The selectivity of Ga₂O₃-based H₂, NO_x, NH₃, CO₂, and VOCs gas sensors is not satisfied due to a strong cross-sensitivity of various target gases. Further improvement of response recovery and long-term stability is also needed for the Ga₂O₃-based NO_x, NH₃, CO₂, and VOCs gas sensors. The noise analyses of Ga₂O₃-based gas sensors have not been explored yet.
- (e) Studies on sensing mechanism and device stability of NO_x, NH₃, CO₂, and VOCs gas sensors are still lack. For instance, studies of the complex nitrite-correlated reactions during the NO_x gas sensing, and of the CO₂ gas sensing on the Ga₂O₃ surface have not been reported yet.
- (f) The trade-off between sensitivity and operation temperature is complex and significantly affected by the activation energy and influence factors. Another trade-off between sensitivity and response speed is determined by the basic gas sensing

mechanism. These trade-offs complicate the improvement of gas sensors performance. The corresponding reports on these trade-offs are rare for Ga_2O_3 -based gas sensors. Further understanding and evaluation of these trade-offs are needed.

In summary, β - Ga_2O_3 gas sensors possess great potentials in applications of detecting oxidizing and reducing gases. Significant progresses have been made in Ga_2O_3 -based O_2 , CO and H_2 gas sensors. In the future, it is necessary to overcome the above-mentioned challenges. The research interests of β - Ga_2O_3 gas sensors may focus on high-performance device, p-type Ga_2O_3 -based sensors, gas sensing mechanisms, novel functionalities, etc. In term of high-performance device, the various-types β - Ga_2O_3 gas sensors with good sensitivity, fast response and recovery, and good selectivity will be developed continuously. The modification of surface morphology and surface/interface properties, and the appropriate doping are useful strategies to modify the growth behavior and material properties to enhance the device performance [123,155–162]. Another useful strategy is the development of functional structures (e.g. van-der-Waals heterostructures, superlattices, mesoporous and ferrite oxides, phononics and photonics crystals, etc.) to improve device performance, and has aroused intense research attentions [138,149,163,164].

P-type oxides are expected to possess more excellent gas sensing properties, and oxide p-n junctions may bring new-design sensors of high-performance gas sensing [15]. Recently, intrinsic weak p-type β - Ga_2O_3 films are achieved by annealing of β - Ga_2O_3 films in oxygen atmosphere [165]. P-type N-doped β - Ga_2O_3 films, fabricated by a novel energy-driven multi-step structural phase transition technique, have been experimentally and theoretically demonstrated with a low acceptor ionization energy, a RT Hall resistivity of $17.0 \Omega\text{cm}$, a Hall hole mobility of $23.6 \text{ cm}^2\text{V}^{-1}\text{s}^{-1}$, and a hole concentration of $1.56 \times 10^{16} \text{ cm}^{-3}$ [22, 24,166]. These recent studies will boost the research of p-type Ga_2O_3 and advance the applications of p-type Ga_2O_3 gas sensors as well as Ga_2O_3 -based power electronic and optoelectronic devices.

Some novel gas sensing phenomena have been observed in recent years. A comprehensive theory to explain the absorption/desorption characteristics of the Ga_2O_3 -based gas sensors should be established, which is significant for the improvement of the device performance. In term of applications, the development of Ga_2O_3 gas sensors with low power consumption, small size, flexibility, etc. is required. The improvement of response recovery and long-term stability is required for the commercialization of Ga_2O_3 -based NO_x , H_2 , NH_3 , VOCs , pH , and humidity gas sensors. In addition, novel functionalities can be extended such as point-of-care diagnosis, monitor-of-person-skin-signal, and so forth.

Declaration of competing interest

The authors declare that they have no known competing financial interests or personal relationships that could have appeared to influence the work reported in this paper.

Acknowledgments

This work was supported by National Natural Science Foundation of China under Grant Nos. 62074039 and 12004074, National Key R&D Program of China (Grant Nos. 2021YFB3601000, 2021YFB3601003), China Postdoctoral Science Foundation under Grant No. 2020M681141, National Postdoctoral Program for Innovative Talents under Grant No. BX20190070.

References

- [1] K. Jamison, J. Eisenhauer, J. Rash, Glass Industry Technology Roadmap, 2002, <https://doi.org/10.2172/1218642>.
- [2] M. Cremer, The cause of the electromotor properties of tissue, and a contribution to the science of polyphasic electrolytes, *Z. Biol.* 29 (1906) 562–608.
- [3] F. Haber, Z. Klemensiewicz, Concerning electrical phase boundary forces, *Z. Phys. Chem.-stochiometrische Verwandtschaftslehre*. 67 (1909) 385–431.
- [4] J. Heyrovský, XXIX. Electrolysis with a dropping mercury cathode. Part I. Deposition of alkali and alkaline earth metals, London, Edinburgh, Dublin Philos. Mag. J. Sci. 45 (1923) 303–315, <https://doi.org/10.1080/14786442308634117>.
- [5] J. Heyrovský, A. Tockstei, Principles OF polarography, *Chem. Listy* 60 (1966) 1636.
- [6] P.T. Moseley, Solid state gas sensors, *Meas. Sci. Technol.* 8 (1997) 223, <https://doi.org/10.1088/0957-0233/8/3/003>.
- [7] A. Gurlo, Nanosensors: towards morphological control of gas sensing activity. SnO_2 , In_2O_3 , ZnO and WO_3 case studies, *Nanoscale* 3 (2011) 154–165, <https://doi.org/10.1039/CN0R00560F>.
- [8] S. Das, V. Jayaraman, SnO_2 : a comprehensive review on structures and gas sensors, *Prog. Mater. Sci.* 66 (2014), <https://doi.org/10.1016/J.PMATSCL.2014.06.003>, 112–255.
- [9] V.S. Bhati, M. Hojaberdiiev, M. Kumar, Enhanced sensing performance of ZnO nanostructures-based gas sensors: a review, *Energy Rep.* 6 (2020) 46–62, <https://doi.org/10.1016/j.egyr.2019.08.070>.
- [10] Z. Li, Z.J. Yao, A.A. Haidry, T. Plecenik, L.J. Xie, L.C. Sun, Q. Fatima, Resistive-type hydrogen gas sensor based on TiO_2 : a review, *Int. J. Hydrogen Energy* 43 (2018) 21114–21132, <https://doi.org/10.1016/J.IJHYDENE.2018.09.051>.
- [11] R. Ahmad, S.M. Majhi, X. Zhang, T.M. Swager, K.N. Salama, Recent progress and perspectives of gas sensors based on vertically oriented ZnO nanomaterials, *Adv. Colloid Interface Sci.* 270 (2019) 1–27, <https://doi.org/10.1016/j.jcis.2019.05.006>.
- [12] T.P. Mokoena, H.C. Swart, D.E. Motaung, A review on recent progress of p-type nickel oxide based gas sensors: future perspectives, *J. Alloys Compd.* 805 (2019) 267–294, <https://doi.org/10.1016/J.JALLCOM.2019.06.329>.
- [13] A. Rydosz, The use of copper oxide thin films in gas-sensing applications, *Coatings* 8 (2018) 425, <https://doi.org/10.3390/COATINGS8120425>.
- [14] J.M. Xu, J.P. Cheng, The advances of Co_3O_4 as gas sensing materials: a review, *J. Alloys Compd.* 686 (2016) 753–768, <https://doi.org/10.1016/J.JALLCOM.2016.06.086>.
- [15] H.J. Kim, J.H. Lee, Highly sensitive and selective gas sensors using p-type oxide semiconductors: Overview, *Sensor. Actuator. B Chem.* 192 (2014) 607–627, <https://doi.org/10.1016/j.snb.2013.11.005>.
- [16] A. Afzal, β - Ga_2O_3 nanowires and thin films for metal oxide semiconductor gas sensors: sensing mechanisms and performance enhancement strategies, *J. Mater.* 5 (2019) 542–557, <https://doi.org/10.1016/j.jmat.2019.08.003>.
- [17] S.J. Pearson, J. Yang, P.H. Cary, F. Ren, J. Kim, M.J. Tadjer, M.A. Mastro, P. H. Cary IV, A review of Ga_2O_3 materials, processing, and devices, *Appl. Phys. Rev.* 5 (2018) 11301–13504, <https://doi.org/10.1063/1.4977857>.
- [18] Shizuo Fujita, Wide-bandgap semiconductor materials: for their full bloom, *Jpn. J. Appl. Phys.* 54 (2015), 030101.
- [19] P. Song, Z. Wu, X. Shen, J. Kang, Z. Fang, T.Y. Zhang, Self-consistent growth of single-crystalline (-01)- β - Ga_2O_3 nanowires using a flexible GaN seed nanocrystal, *CrysEngComm* 19 (2017) 625–631, <https://doi.org/10.1039/c6ce02319c>.
- [20] Z. Wu, Z. Jiang, P. Song, P. Tian, L. Hu, R. Liu, Z. Fang, J. Kang, T.Y. Zhang, Nanowire-seeded growth of single-crystalline (010) β - Ga_2O_3 nanosheets with high field-effect electron mobility and on/off current ratio, *Small* 15 (2019) 2–7, <https://doi.org/10.1002/smll.201900580>.
- [21] E.B. Yakimov, A.Y. Polyakov, I.V. Shchemberov, N.B. Smirnov, A.A. Vasilev, A. I. Kochkova, P.S. Vergeles, E.E. Yakimov, A.V. Chernykh, M. Xian, F. Ren, S. J. Pearson, On the nature of photosensitivity gain in Ga_2O_3 Schottky diode detectors: effects of hole trapping by deep acceptors, *J. Alloys Compd.* 879 (2021), 160394, <https://doi.org/10.1016/J.JALLCOM.2021.160394>.
- [22] Z.X. Jiang, Z.Y. Wu, C.C. Ma, J.N. Deng, H. Zhang, Y. Xu, J.D. Ye, Z.L. Fang, G. Q. Zhang, J.Y. Kang, T.Y. Zhang, P-type β - Ga_2O_3 metal-semiconductor-metal solar-blind photodetectors with extremely high responsivity and gain-bandwidth product, *Mater. Today Phys.* 14 (2020), 100226, <https://doi.org/10.1016/j.mtphys.2020.100226>.
- [23] Y. Lv, H. Liu, X. Zhou, Y. Wang, X. Song, Y. Cai, Q. Yan, C. Wang, S. Liang, J. Zhang, Z. Feng, H. Zhou, S. Cai, Y. Hao, Lateral β - Ga_2O_3 MOSFETs with high power figure of merit of 277 MW/cm^2 , *IEEE Electron. Device Lett.* 41 (2020) 537–540, <https://doi.org/10.1109/LED.2020.2974515>.
- [24] Z.Y. Wu, Z.X. Jiang, C.C. Ma, W. Ruan, Y. Chen, H. Zhang, G.Q. Zhang, Z.L. Fang, J.Y. Kang, T.Y. Zhang, Energy-driven multi-step structural phase transition mechanism to achieve high-quality p-type nitrogen-doped β - Ga_2O_3 films, *Mater. Today Phys.* 17 (2021), 100356, <https://doi.org/10.1016/j.mtphys.2021.100356>.
- [25] W. Ruan, Z. Wu, J. Liu, J. Chen, Y. Shan, P. Song, Z. Jiang, R. Liu, G. Zhang, Z. Fang, β - Ga_2O_3 nanowires: controlled growth, characterization, and deep-ultraviolet photodetection application, *J. Phys. D Appl. Phys.* 55 (2022), 284001, <https://doi.org/10.1088/1361-6463/ac66a5>.
- [26] H. Ji, W. Zeng, Y. Li, Gas sensing mechanisms of metal oxide semiconductors: a focus review, *Nanoscale* 11 (2019) 22664–22684, <https://doi.org/10.1039/c9nr07699a>.
- [27] P.T. Moseley, Materials selection for semiconductor gas sensors, *Sensor. Actuator. B Chem.* 6 (1992) 149–156, [https://doi.org/10.1016/0925-4005\(92\)80047-2](https://doi.org/10.1016/0925-4005(92)80047-2).
- [28] V. Brynzari, G. Korotchenkov, S. Dmitriev, Theoretical study of semiconductor thin films gas sensors. Attempt to consistent approach, *Electron. Technol.* 33 (2000) 225–235.
- [29] U. Hoefer, J. Frank, M. Fleischer, High temperature Ga_2O_3 -gas sensors and SnO_2 -gas sensors: a comparison, *Sensor. Actuator. B Chem.* 78 (2001) 6–11, [https://doi.org/10.1016/S0925-4005\(01\)00784-5](https://doi.org/10.1016/S0925-4005(01)00784-5).

- [30] I. Sayago, J. Getino, Hall effect measurements to calculate the conduction control in semiconductor films of SnO_2 , *Sens. Actuators, A* 4142 (1994) 619–621.
- [31] I. Lundström, Hydrogen sensitive mos-structures: Part 1: principles and applications, *Sens. Actuators, A* 1 (1981) 403–426, [https://doi.org/10.1016/0250-6874\(81\)80018-2](https://doi.org/10.1016/0250-6874(81)80018-2).
- [32] I. Lundström, D. Söderberg, Hydrogen sensitive mos-structures part 2: characterization, *Sens. Actuators, A* 2 (1981) 105–138, [https://doi.org/10.1016/0250-6874\(81\)80032-7](https://doi.org/10.1016/0250-6874(81)80032-7).
- [33] N. Bärsan, M. Hübner, U. Weimar, Conduction mechanisms in SnO_2 based polycrystalline thick film gas sensors exposed to CO and H_2 in different oxygen backgrounds, *Sensor. Actuator. B Chem.* 157 (2011) 510–517, <https://doi.org/10.1016/J.SN.2011.05.011>.
- [34] X. Wang, Y. Wang, F. Tian, H. Liang, K. Wang, X. Zhao, Z. Lu, K. Jiang, L. Yang, X. Lou, From the surface reaction control to gas-diffusion control: the synthesis of hierarchical porous SnO_2 microspheres and their gas-sensing mechanism, *J. Phys. Chem. C* 119 (2015) 15963–15976, https://doi.org/10.1021/ACS.JPCC.5B01397.SUPPLFILE/JP5B01397_SI_001.PDF.
- [35] N.S. Ramgir, S.K. Ganapathi, M. Kaur, N. Datta, K.P. Muthe, D.K. Aswal, S. K. Gupta, J.V. Yakhmi, Sub-ppm H_2S sensing at room temperature using CuO thin films, *Sensor. Actuator. B Chem.* 151 (2010) 90–96, <https://doi.org/10.1016/J.SN.2010.09.043>.
- [36] J. Ming, Y. Wu, L. Wang, Y. Yu, F. Zhao, CO_2 -assisted template synthesis of porous hollow bi-phase γ - α - Fe_2O_3 nanoparticles with high sensor property, *J. Mater. Chem.* 21 (2011) 17776–17782, <https://doi.org/10.1039/C1JM12879E>.
- [37] G. Gao, J. Wu, G. Wu, Z. Zhang, W. Feng, J. Shen, B. Zhou, Phase transition effect on durability of WO_3 hydrogen sensing films: an insight by experiment and first-principle method, *Sensor. Actuator. B Chem.* 171–172 (2012) 1288–1291, <https://doi.org/10.1016/J.SN.2012.06.028>.
- [38] J. He, X. Rao, C. Yang, J. Wang, X. Su, C. Niu, Glucose-assisted synthesis of mesoporous maghemite nanoparticles with enhanced gas sensing properties, *Sensor. Actuator. B Chem.* 201 (2014) 213–221, <https://doi.org/10.1016/J.SN.2014.04.053>.
- [39] F.E. Annanouch, Z. Haddi, S. Vallejos, P. Umek, P. Guttmann, C. Bittencourt, E. Llobet, Aerosol-assisted CVD-grown WO_3 nanoneedles decorated with copper oxide nanoparticles for the selective and humidity-resilient detection of H_2S , *ACS Appl. Mater. Interfaces* 7 (2015) 6842–6851, https://doi.org/10.1021/ACSAM1.5B00411.SUPPLFILE/AM5B00411_SI_001.PDF.
- [40] M. Wang, T. Hou, Z. Shen, X. Zhao, H. Ji, MOF-derived Fe_2O_3 : phase control and effects of phase composition on gas sensing performance, *Sensor. Actuator. B Chem.* 292 (2019) 171–179, <https://doi.org/10.1016/J.SN.B.2019.04.124>.
- [41] M. Ikram, H. Lv, Z. Liu, K. Shi, Y. Gao, Hydrothermally derived p-n MoS_2 - ZnO from p-p MoS_2 -ZIF-8 for an efficient detection of NO_2 at room temperature, *J. Mater. Chem. A* 9 (2021) 14722–14730, <https://doi.org/10.1039/DITA03578A>.
- [42] C. Guo, X. Dong, X. Zhang, X. Cheng, Q. Li, Y. Sun, W. Liu, L. Huo, Y. Xu, Controllable construction of Ho_2O_3 nanomaterials with different dimensions (1D, 2D, and 3D) for real-time monitoring human breathing and body surface humidity detection, *J. Mater. Chem. A* 9 (2021) 11632–11640, <https://doi.org/10.1039/DITA00631B>.
- [43] T. Schwebel, M. Fleischer, H. Meixner, Selective, temperature compensated O_2 sensor based on Ga_2O_3 thin films, *Sensor. Actuator. B Chem.* 65 (2000) 176–180, [https://doi.org/10.1016/S0925-4005\(99\)00326-3](https://doi.org/10.1016/S0925-4005(99)00326-3).
- [44] Z. Liu, T. Yamazaki, Y. Shen, T. Kikuta, N. Nakatani, Y. Li, O_2 and CO sensing of Ga_2O_3 multiple nanowire gas sensors, *Sensor. Actuator. B Chem.* 129 (2008) 666–670, <https://doi.org/10.1016/j.snb.2007.09.055>.
- [45] Q.N. Abdullah, A.R. Ahmed, A.M. Ali, F.K. Yam, Z. Hassan, M. Bououdina, Novel SnO_2 -coated β - Ga_2O_3 nanostructures for room temperature hydrogen gas sensor, *Int. J. Hydrogen Energy* 46 (2021) 7000–7010, <https://doi.org/10.1016/J.IJHYDENE.2020.11.109>.
- [46] R. Pandeeswari, B.G. Jeyaprakash, High sensing response of β - Ga_2O_3 thin film towards ammonia vapours: influencing factors at room temperature, *Sensor. Actuator. B Chem.* 195 (2014) 206–214, <https://doi.org/10.1016/j.snb.2014.01.025>.
- [47] K. Dyndal, A. Zarzycki, W. Andrysiewicz, D. Grochala, K. Marszalek, A. Rydosz, $\text{CuO-Ga}_2\text{O}_3$ thin films as a gas-sensitive material for acetone detection, *Sensors* 20 (2020), <https://doi.org/10.3390/s20113142>.
- [48] J. Wang, S. Jiang, H. Liu, S. Wang, Q. Pan, Y. Yin, G. Zhang, P-type gas-sensing behavior of $\text{Ga}_2\text{O}_3/\text{Al}_2\text{O}_3$ nanocomposite with high sensitivity to NO_x at room temperature, *J. Alloys Compd.* 814 (2020), 152284, <https://doi.org/10.1016/j.jallcom.2019.152284>.
- [49] M. Fleischer, H. Meixner, A selective CH_4 sensor using semiconducting Ga_2O_3 thin films based on temperature switching of multigas reactions, *Sensor. Actuator. B Chem.* 25 (1995) 544–547, [https://doi.org/10.1016/0925-4005\(95\)85118-6](https://doi.org/10.1016/0925-4005(95)85118-6).
- [50] J. Frank, M. Fleischer, H. Meixner, Gas-sensitive electrical properties of pure and doped semiconducting Ga_2O_3 thick films, *Sensor. Actuator. B Chem.* 48 (1998) 318–321, [https://doi.org/10.1016/S0925-4005\(98\)00064-1](https://doi.org/10.1016/S0925-4005(98)00064-1).
- [51] Y.M. Juan, S.J. Chang, H.T. Hsueh, S.H. Wang, W.Y. Weng, T.C. Cheng, C.L. Wu, Effects of humidity and ultraviolet characteristics on β - Ga_2O_3 nanowire sensor, *RSC Adv.* 5 (2015) 84776–84781, <https://doi.org/10.1039/c5ra16710h>.
- [52] P. Feng, X.Y. Xue, Y.G. Liu, Q. Wan, T.H. Wang, Achieving fast oxygen response in individual β - Ga_2O_3 nanowires by ultraviolet illumination, *Appl. Phys. Lett.* 89 (2006), 112114, <https://doi.org/10.1063/1.2349278>.
- [53] S. An, S. Park, Y. Mun, C. Lee, UV enhanced NO_2 sensing properties of Pt functionalized Ga_2O_3 nanorods, *Bull. Kor. Chem. Soc.* 34 (2013) 1632–1636, <https://doi.org/10.5012/bkcs.2013.34.6.1632>.
- [54] H.J. Lin, H. Gao, P.X. Gao, UV-enhanced CO sensing using Ga_2O_3 -based nanorod arrays at elevated temperature, *Appl. Phys. Lett.* 110 (2017), 043101, <https://doi.org/10.1063/1.4974213>.
- [55] M. Fleischer, H. Meixner, Oxygen sensing with long-term stable Ga_2O_3 thin films, *Sensor. Actuator. B Chem.* 5 (1991) 115–119, [https://doi.org/10.1016/0925-4005\(91\)80230-H](https://doi.org/10.1016/0925-4005(91)80230-H).
- [56] M. Fleischer, H. Meixner, Gallium oxide thin films: a new material for high-temperature oxygen sensors, *Sensor. Actuator. B Chem.* 4 (1991) 437–441, [https://doi.org/10.1016/0925-4005\(91\)80148-D](https://doi.org/10.1016/0925-4005(91)80148-D).
- [57] M. Bartic, Mechanism of oxygen sensing on β - Ga_2O_3 single-crystal sensors for high temperatures, *Phys. Status Solidi* 213 (2016) 457–462, <https://doi.org/10.1002/pssa.201532599>.
- [58] Y. Li, A. Trinchi, W. Włodarski, K. Galatsis, K. Kalantar-Zadeh, Investigation of the oxygen gas sensing performance of Ga_2O_3 thin films with different dopants, *Sensor. Actuator. B Chem.* 93 (2003) 431–434, [https://doi.org/10.1016/S0925-4005\(03\)00171-0](https://doi.org/10.1016/S0925-4005(03)00171-0).
- [59] S. Manandhar, A.K. Battu, A. Devaraj, V. Shutthanandan, S. Thevuthasan, C. V. Ramana, Rapid response high temperature oxygen sensor based on titanium doped gallium oxide, *Sci. Rep.* 10 (2020) 178, <https://doi.org/10.1038/s41598-019-54136-8>.
- [60] A.V. Almaev, E.V. Chernikov, N.A. Davletkildeev, D.V. Sokolov, Oxygen sensors based on gallium oxide thin films with addition of chromium, *Superlattice. Microst.* 139 (2020), 106392, <https://doi.org/10.1016/j.spmi.2020.106392>.
- [61] L.T. Ju, S.L. Ju, Deposition of Ga_2O_3 thin film for high-temperature oxygen sensing applications, *J. Ovonics Res.* 8 (2012) 73–79.
- [62] M. Bartic, M. Ogita, M. Isai, C.L. Baban, H. Suzuki, Oxygen sensing properties at high temperatures of β - Ga_2O_3 thin films deposited by the chemical solution deposition method, *J. Appl. Phys.* 102 (2007), <https://doi.org/10.1063/1.2756085>.
- [63] C. Baban, Y. Toyoda, M. Ogita, Oxygen sensing at high temperatures using Ga_2O_3 films, *Thin Solid Films* 484 (2005) 369–373, <https://doi.org/10.1016/j.tsf.2005.03.001>.
- [64] C. Malagù, V. Guidi, M. Stefancich, M.C. Carotta, G. Martinelli, Model for Schottky barrier and surface states in nanostructured n-type semiconductors, *J. Appl. Phys.* 91 (2001) 808, <https://doi.org/10.1063/1.1425434>.
- [65] C.H. Wu, G.J. Jiang, K.W. Chang, Z.Y. Deng, K.L. Chen, Amorphous indium gallium zinc oxide thin film-based ozone sensors, in: 2015 IEEE SENSORS - Proc., Institute of Electrical and Electronics Engineers Inc., 2015, <https://doi.org/10.1109/ICSENS.2015.7370578>.
- [66] Y. Sui, H. Liang, Q. Chen, W. Huo, X. Du, Z. Mei, Room-temperature ozone sensing capability of IGZO-decorated amorphous Ga_2O_3 films, *ACS Appl. Mater. Interfaces* 12 (2020) 8929–8934, <https://doi.org/10.1021/acsm.9b22400>.
- [67] N. Sui, P. Zhang, T. Zhou, T. Zhang, Selective ppb-level ozone gas sensor based on hierarchical branch-like In_2O_3 nanostructure, *Sensor. Actuator. B Chem.* 336 (2021), 129612, <https://doi.org/10.1016/J.SN.B.2021.129612>.
- [68] J. Frank, M. Fleischer, M. Zimmer, H. Meixner, Ozone sensing using In_2O_3 -modified Ga_2O_3 thin films, *IEEE Sensor. J.* 1 (2001) 318–321.
- [69] G. Korotcenkov, V. Brinzari, V. Golovanov, Y. Blinov, Kinetics of gas response to reducing gases of SnO_2 films, deposited by spray pyrolysis, *Sensor. Actuator. B Chem.* 98 (2004) 41–45, <https://doi.org/10.1016/J.SN.B.2003.08.022>.
- [70] M. Fleischer, H. Meixner, Electron mobility in single- and polycrystalline Ga_2O_3 , *J. Appl. Phys.* 74 (1998) 300, <https://doi.org/10.1063/1.354107>.
- [71] G. Korotcenkov, V. Brinzari, V. Golovanov, A. Cerneavski, V. Matolin, A. Tadd, Acceptor-like behavior of reducing gases on the surface of n-type In_2O_3 , *Appl. Surf. Sci.* 227 (2004) 122–131, <https://doi.org/10.1016/JAPSUSC.2003.11.051>.
- [72] G. Korotcenkov, M. Ivanov, I. Blinov, J.R. Stetter, Kinetics of indium oxide-based thin film gas sensor response: the role of “redox” and adsorption/desorption processes in gas sensing effects, *Thin Solid Films* 515 (2007) 3987–3996, <https://doi.org/10.1016/J.TSF.2006.09.044>.
- [73] K. Wang, H. Ren, Z. Wang, J. Wei, Temperature-pressure coupling effect on gas desorption characteristics in coal during low-variable temperature process, *J. Petrol. Sci. Eng.* 211 (2022), 110104, <https://doi.org/10.1016/J.PETROL.2022.110104>.
- [74] T. Krishnakumar, R. Jayaprakash, N. Pinna, N. Donato, A. Bonavita, G. Micali, G. Neri, CO gas sensing of ZnO nanostructures synthesized by an assisted microwave wet chemical route, *Sensor. Actuator. B Chem.* 143 (2009) 198–204, <https://doi.org/10.1016/J.SN.B.2009.09.039>.
- [75] N.D. Khoang, H.S. Hong, D.D. Trung, N. Van Duy, N.D. Hoa, D.D. Thinh, N. Van Hieu, On-chip growth of wafer-scale planar-type ZnO nanorod sensors for effective detection of CO gas, *Sensor. Actuator. B Chem.* 181 (2013) 529–536, <https://doi.org/10.1016/J.SN.B.2013.02.047>.
- [76] S. Mahajan, S. Jagtap, Metal-oxide semiconductors for carbon monoxide (CO) gas sensing: a review, *Appl. Mater. Today* 18 (2020), 100483, <https://doi.org/10.1016/J.APMT.2019.100483>.
- [77] N. Vorobyeva, M. Rumyantseva, V. Platonov, D. Filatova, A. Chizhov, A. Marikutsa, I. Bozhev, A. Gaskov, $\text{Ga}_2\text{O}_3(\text{Sn})$ oxides for high-temperature gas sensors, *Nanomaterials* 11 (2021) 2938, <https://doi.org/10.3390/NANO1112938>.
- [78] N. Wu, Z. Chen, J. Xu, M. Chyu, S.X. Mao, Impedance-metric Pt/YSZ/Au- Ga_2O_3 sensor for CO detection at high temperature, *Sensor. Actuator. B Chem.* 110 (2005) 49–53, <https://doi.org/10.1016/j.snb.2005.01.012>.
- [79] A. Marsal, A. Cornet, J.R. Morante, Study of the CO and humidity interference in La doped tin oxide CO_2 gas sensor, *Sensor. Actuator. B Chem.* 94 (2003) 324–329, [https://doi.org/10.1016/S0925-4005\(03\)00461-1](https://doi.org/10.1016/S0925-4005(03)00461-1).

- [80] Y. Lin, Z. Fan, Compositing strategies to enhance the performance of chemiresistive CO₂ gas sensors, *Mater. Sci. Semicond. Process.* 107 (2020), 104820, <https://doi.org/10.1016/J.MSSP.2019.104820>.
- [81] H. Ogawa, M. Nishikawa, A. Abe, Hall measurement studies and an electrical conduction model of tin oxide ultrafine particle films, *J. Appl. Phys.* 53 (1982) 4448, <https://doi.org/10.1063/1.331230>.
- [82] P.K. Kannan, R. Saraswathi, J.B.B. Rayappan, CO₂ gas sensing properties of DC reactive magnetron sputtered ZnO thin film, *Ceram. Int.* 40 (2014) 13115–13122, <https://doi.org/10.1016/J.CERAMINT.2014.05.011>.
- [83] H. Kim, C. Jin, S. An, C. Lee, Fabrication and CO gas-sensing properties of Pt-functionalized Ga₂O₃ nanowires, *Ceram. Int.* 38 (2012) 3563–3567, <https://doi.org/10.1016/j.ceramint.2011.12.072>.
- [84] T.F. Weng, M.S. Ho, C. Sivakumar, B. Balraj, P.F. Chung, VLS growth of pure and Au decorated β -Ga₂O₃ nanowires for room temperature CO gas sensor and resistive memory applications, *Appl. Surf. Sci.* 533 (2020), 147476, <https://doi.org/10.1016/j.apsusc.2020.147476>.
- [85] G. Neri, A. Bonavita, C. Milone, S. Galvagno, Role of the Au oxidation state in the CO sensing mechanism of Au/iron oxide-based gas sensors, *Sensor. Actuator. B Chem.* 93 (2003) 402–408, [https://doi.org/10.1016/S0925-4005\(03\)00188-6](https://doi.org/10.1016/S0925-4005(03)00188-6).
- [86] S.H. Park, S.H. Kim, S.Y. Park, C. Lee, Synthesis and CO gas sensing properties of surface-nitridated Ga₂O₃ nanowires, *RSC Adv.* 4 (2014) 63402–63407, <https://doi.org/10.1039/c4ra09538c>.
- [87] P. Karnati, S. Akbar, P.A. Morris, Conduction mechanisms in one dimensional core-shell nanostructures for gas sensing: a review, *Sensor. Actuator. B Chem.* 295 (2019) 127–143, <https://doi.org/10.1016/j.snb.2019.05.049>.
- [88] Q.C. Bui, L. Largeau, M. Morassi, N. Jegenyes, O. Mauguin, L. Travers, X. Lafosse, C. Dupuis, J.-C. Harmand, M. Tchernycheva, N. Gogneau, GaN/Ga₂O₃ core/shell nanowires growth: towards high response gas sensors, *Appl. Sci.* 9 (2019) 3528, <https://doi.org/10.3390/app9173528>.
- [89] H.J. Lin, J.P. Baltrus, H. Gao, Y. Ding, C.Y. Nam, P. Ohodnicki, P.X. Gao, Perovskite nanoparticle-sensitized Ga₂O₃ nanorod arrays for CO detection at high temperature, *ACS Appl. Mater. Interfaces* 8 (2016) 8880–8887, <https://doi.org/10.1021/acsami.6b01709>.
- [90] S. Yan, L. Wan, Z. Li, Y. Zhou, Z. Zou, Synthesis of a mesoporous single crystal Ga₂O₃ nanoplate with improved photoluminescence and high sensitivity in detecting CO, *Chem. Commun.* 46 (2010) 6388–6390, <https://doi.org/10.1039/c0cc01579b>.
- [91] K. Girija, S. Thirumalairajan, V.R. Mastelaro, D. Mangalaraj, Catalyst free vapor-solid deposition of morphologically different β -Ga₂O₃ nanostructure thin films for selective CO gas sensors at low temperature, *Anal. Methods* 8 (2016) 3224–3235, <https://doi.org/10.1039/c6ay00391c>.
- [92] M. Bagheri, A.A. Khodadadi, A.R. Mahjoub, Y. Mortazavi, Strong effects of gallia on structure and selective responses of Ga₂O₃-In₂O₃ nanocomposite sensors to either ethanol, CO or CH₄, *Sensor. Actuator. B Chem.* 220 (2015) 590–599, <https://doi.org/10.1016/j.snb.2015.06.007>.
- [93] M. Fleischer, H. Meixner, Sensing reducing gases at high temperatures using long-term stable Ga₂O₃ thin films, *Sensor. Actuator. B Chem.* 6 (1992) 257–261, [https://doi.org/10.1016/0925-4005\(92\)80065-6](https://doi.org/10.1016/0925-4005(92)80065-6).
- [94] A. Afzal, N. Cioffi, L. Sabbatini, L. Torsi, NO_x sensors based on semiconducting metal oxide nanostructures: progress and perspectives, *Sensor. Actuator. B Chem.* 171–172 (2012) 25–42, <https://doi.org/10.1016/j.snb.2012.05.026>.
- [95] M. Hai-Lin, F. Duo-Wang, N. Xiao-Shan, Preparation and NO₂-gas sensing property of individual β -Ga₂O₃ nanobelt, *Chin. Phys. B* 19 (2010), 76102.
- [96] B. Zhang, H.J. Lin, H. Gao, X. Lu, C.Y. Nam, P.X. Gao, Perovskite-sensitized β -Ga₂O₃ nanorod arrays for highly selective and sensitive NO₂ detection at high temperature, *J. Mater. Chem. A* 8 (2020) 10845–10854, <https://doi.org/10.1039/d0ta02691c>.
- [97] C. Jin, S. Park, H. Kim, C. Lee, Ultrasensitive multiple networked Ga₂O₃-core/ZnO-shell nanorod gas sensors, *Sensor. Actuator. B Chem.* 161 (2012) 223–228, <https://doi.org/10.1016/j.snb.2011.10.023>.
- [98] S. Park, H. Kim, C. Jin, C. Lee, Synthesis, structure, and room-temperature gas sensing of multiple-networked Pd-doped Ga₂O₃ nanowires, *J. Kor. Phys. Soc.* 60 (2012) 1560–1564, <https://doi.org/10.3938/kps.60.1560>.
- [99] H.W. Zan, C.H. Li, C.C. Yeh, M.Z. Dai, H.F. Meng, C.C. Tsai, Room-temperature-operated sensitive hybrid gas sensor based on amorphous indium gallium zinc oxide thin-film transistors, *Appl. Phys. Lett.* 98 (2011), 253503, <https://doi.org/10.1063/1.3601488>.
- [100] D.J. Yang, G.C. Whitfield, N.G. Cho, P.S. Cho, I.D. Kim, H.M. Saltsburg, H. L. Tuller, Amorphous InGaZnO₄ films: gas sensor response and stability, *Sensor. Actuator. B Chem.* 171–172 (2012) 1166–1171, <https://doi.org/10.1016/j.snb.2012.06.057>.
- [101] S.B. Eadi, H.J. Shin, K.W. Song, H.W. Choi, S.H. Kim, H.D. Lee, Development of ultrasensitive indium oxide layer with high response to NO₂ gas in indium gallium zinc oxide stack structure using atomic layer deposition, *Mater. Lett.* 297 (2021), 129943, <https://doi.org/10.1016/J.MATLET.2021.129943>.
- [102] T.L. Guidotti, The higher oxides of nitrogen: inhalation toxicology, *Environ. Res.* 15 (1978) 443–472, [https://doi.org/10.1016/0013-9351\(78\)90125-1](https://doi.org/10.1016/0013-9351(78)90125-1).
- [103] A. Richters, K. Kuraitis, Inhalation of NO₂ and blood borne cancer cell spread to the lungs, *Arch. Environ. Health* 36 (1981) 36–39, <https://doi.org/10.1080/00039896.1981.10667604>.
- [104] S.A. Kharitonov, P.J. Barnes, Exhaled markers of pulmonary disease, *Am. J. Respir. Crit. Care Med.* 163 (2001) 1693–1722, <https://doi.org/10.1164/AJRCCM.163.7.2009041>.
- [105] R.A. Dweik, S.A.A. Comhair, B. Gaston, F.B.J.M. Thunnissen, C. Farver, M. J. Thomassen, M. Kavuru, J. Hammel, H.M. Abu-Soud, S.C. Erzurum, NO chemical events in the human airway during the immediate and late antigen-induced asthmatic response, *Proc. Natl. Acad. Sci. U. S. A* 98 (2001) 2622–2627, <https://doi.org/10.1073/PNAS.051629498/ASSET/1706996F-A92C-41C3-81D9-1F8955847802/ASSETS/GRAFIC/PQ0516294004.JPG>.
- [106] M. Machida, H. Murakami, T. Kitsubayashi, T. Kijima, NO-intercalation properties of a double-layered cuprate, La_{2-x}Ba_xSrCu₂O₆. Dissociative desorption of intercalated NO, *Chem. Mater.* 9 (1997) 135–140, <https://doi.org/10.1021/CM960254C>.
- [107] J.J. Yu, Z. Jiang, L. Zhu, Z.P. Hao, Z.P. Xu, Adsorption/desorption studies of NO_x on well-mixed oxides derived from Co-Mg/Al hydrotalcite-like compounds, *J. Phys. Chem. B* 110 (2006) 4291–4300, <https://doi.org/10.1021/JP056473F>.
- [108] B. Azambre, L. Zenbourn, A. Koch, J.V. Weber, Adsorption and desorption of NO_x on commercial ceria-zirconia (Ce_xZr_{1-x}O₂) mixed oxides: a combined TGA, TPD-MS, and DRIFTS study, *J. Phys. Chem. C* 113 (2009) 13287–13299, https://doi.org/10.1021/JP9008674/ASSET/IMAGES/MEDIUM/JP-2009-008674_0008.GIF.
- [109] S. Goldstein, D. Behar, T. Rajh, J. Rabani, Nitrite reduction to nitrous oxide and ammonia by TiO₂ electrons in a colloid solution via consecutive one-electron transfer reactions, *J. Phys. Chem. A* 120 (2016) 2307–2312, https://doi.org/10.1021/ACS.JPCA.6B01761/SUPPL_FILE/JP6B01761_SI_001.PDF.
- [110] Q. Zhang, Z. Pang, W. Hu, J. Li, Y. Liu, Y. Liu, F. Yu, C. Zhang, M. Xu, Performance degradation mechanism of the light-activated room temperature NO₂ gas sensor based on Ag-ZnO nanoparticles, *Appl. Surf. Sci.* 541 (2021), 148418, <https://doi.org/10.1016/J.APSUSC.2020.148418>.
- [111] Y. Han, D. Huang, Y. Ma, G. He, J. Hu, J. Zhang, N. Hu, Y. Su, Z. Zhou, Y. Zhang, Z. Yang, Design of hetero-nanostructures on MoS₂ nanosheets to boost NO₂ room-temperature sensing, *ACS Appl. Mater. Interfaces* 10 (2018) 22640–22649, https://doi.org/10.1021/ACSAMI.8B05811/SUPPL_FILE/AM8B05811_SI_001.PDF.
- [112] X. Chen, J. Hu, P. Chen, M. Yin, F. Meng, Y. Zhang, UV-light-assisted NO₂ gas sensor based on WS₂/PbS heterostructures with full recoverability and reliable anti-humidity ability, *Sensor. Actuator. B Chem.* 339 (2021), 129902, <https://doi.org/10.1016/J.SNB.2021.129902>.
- [113] R.S. Wagner, W.C. Ellis, Vapor-liquid-solid mechanism of single crystal growth, *Appl. Phys. Lett.* 4 (1964) 89–90, <https://doi.org/10.1063/1.1753975>.
- [114] H. Li, Z. Gao, W. Lin, W. He, J. Li, Y. Yang, Improving the sensitive property of graphenebased gas sensor by illumination and heating, *Sens. Rev.* 37 (2017) 142–146, <https://doi.org/10.1108/SR-09-2016-0168>.
- [115] W. Jiang, T. Wang, X. Chen, B. Li, M. Zeng, N. Hu, Y. Su, Z. Zhou, Y. Zhang, Z. Yang, Enhancing room-temperature NO₂ detection of cobalt phthalocyanine based gas sensor at an ultralow laser exposure, *Phys. Chem. Chem. Phys.* 22 (2020) 18499–18506, <https://doi.org/10.1039/d0cp02093a>.
- [116] V.P. Verma, S. Das, S. Hwang, H. Choi, M. Jeon, W. Choi, Nitric oxide gas sensing at room temperature by functionalized single zinc oxide nanowire, *Mater. Sci. Eng. B* 171 (2010) 45–49, <https://doi.org/10.1016/J.MSEB.2010.03.066>.
- [117] R. Wagner, D. Schönauer-Kämin, R. Moos, Novel operation strategy to obtain a fast gas sensor for continuous ppb-level NO₂ detection at room temperature using ZnO—a concept study with experimental proof, *Sensors* 19 (2019) 4104, <https://doi.org/10.3390/S19194104>.
- [118] Y. Chen, Z. Liu, J. Li, X. Cheng, J. Ma, H. Wang, D. Li, Robust interlayer coupling in two-dimensional perovskite/monolayer transition metal dichalcogenide heterostructures, *ACS Nano* 14 (2020) 10258–10264, https://doi.org/10.1021/ACSNANO.0C03624/SUPPL_FILE/NN0C03624_SI_001.PDF.
- [119] A.I. Manilov, V.A. Skryshevsky, Hydrogen in porous silicon — a review, *Mater. Sci. Eng. B* 178 (2013) 942–955, <https://doi.org/10.1016/J.MSEB.2013.05.001>.
- [120] M.A.H. Khan, M.V. Rao, Gallium nitride (GaN) nanostructures and their gas sensing properties: a review, *Sensors* 20 (2020) 3889, <https://doi.org/10.3390/S20143889>.
- [121] J.S. Wright, W. Lim, D.P. Norton, S.J. Pearton, F. Ren, J.L. Johnson, A. Ural, Nitride and oxide semiconductor nanostructured hydrogen gas sensors, *Semicond. Sci. Technol.* 25 (2010), 024002, <https://doi.org/10.1088/0268-1242/25/2/024002>.
- [122] G. Brezeanu, M. Badila, F. Draghici, R. Pascu, G. Pristavu, F. Craciunoiu, I. Rusu, High temperature sensors based on silicon carbide (SiC) devices, in: 2015 Int. Semiconf. Conf., IEEE, 2015, pp. 3–10, <https://doi.org/10.1109/SMICND.2015.7355147>.
- [123] J.E.N. Swallow, J.B. Varley, L.A.H. Jones, J.T. Gibbon, L.F.J. Piper, V.R. Dhanak, T.D. Veal, Transition from electron accumulation to depletion at β -Ga₂O₃ surfaces: the role of hydrogen and the charge neutrality level, *Apl. Mater.* 7 (2019), 022528, <https://doi.org/10.1063/1.5054091>.
- [124] Y.X. Pan, D. Mei, C.J. Liu, Q. Ge, Hydrogen adsorption on Ga₂O₃ surface: a combined experimental and computational study, *J. Phys. Chem. C* 115 (2011) 10140–10146, https://doi.org/10.1021/JP2014226/ASSET/IMAGES/MEDIUM/JP-2011-014226_0008.GIF.
- [125] J. Haber, M. Witko, Oxidation catalysis—electronic theory revisited, *J. Catal.* 216 (2003) 416–424, [https://doi.org/10.1016/S0021-9517\(02\)00037-4](https://doi.org/10.1016/S0021-9517(02)00037-4).
- [126] C.T. Lee, J.T. Yan, Sensing mechanisms of Pt/ β -Ga₂O₃/GaN hydrogen sensor diodes, *Sensor. Actuator. B Chem.* 147 (2010) 723–729, <https://doi.org/10.1016/J.SNB.2010.04.008>.
- [127] N.H. Nickel, K. Geilert, Hydrogen density-of-states distribution in β -Ga₂O₃, *J. Appl. Phys.* 129 (2021), 195704, <https://doi.org/10.1063/5.0030903>.
- [128] M. Fleischer, H. Meixner, Improvements in Ga₂O₃ sensors for reducing gases, *Sensor. Actuator. B Chem.* 13 (1993) 259–263, [https://doi.org/10.1016/0925-4005\(93\)85376-L](https://doi.org/10.1016/0925-4005(93)85376-L).
- [129] F. Réti, M. Fleischer, H. Meixner, J. Giber, Effect of coadsorption of reducing gases on the conductivity of β -Ga₂O₃ thin films in the presence of O₂, *Sensor. Actuator. B Chem.* 19 (1994) 573–577, [https://doi.org/10.1016/0925-4005\(93\)01157-Y](https://doi.org/10.1016/0925-4005(93)01157-Y).

- [130] J.T. Yan, C.T. Lee, Improved detection sensitivity of Pt/ β -Ga₂O₃/GaN hydrogen sensor diode, *Sensor. Actuator. B Chem.* 143 (2009) 192–197, <https://doi.org/10.1016/j.snb.2009.08.040>.
- [131] J. Deng, W. Zhu, O.K. Tan, X. Yao, Amorphous Pb(Zr, Ti)O₃ thin film hydrogen gas sensor, *Sensor. Actuator. B Chem.* 77 (2001) 416–420, [https://doi.org/10.1016/S0925-4005\(01\)00707-9](https://doi.org/10.1016/S0925-4005(01)00707-9).
- [132] N.D. Cuong, Y.W. Park, S.G. Yoon, Microstructural and electrical properties of Ga₂O₃ nanowires grown at various temperatures by vapor-liquid-solid technique, *Sensor. Actuator. B Chem.* 140 (2009) 240–244, <https://doi.org/10.1016/j.snb.2009.04.020>.
- [133] S. Jang, S. Jung, J. Kim, F. Ren, S.J. Pearton, K.H. Baik, Hydrogen sensing characteristics of Pt Schottky diodes on (-201) and (010) Ga₂O₃ single crystals, *ECS J. Solid State Sci. Technol.* 7 (2018) Q3180–Q3182, <https://doi.org/10.1149/2.0261807jss>.
- [134] A.V. Almaev, V.I. Nikolaev, N.N. Yakovlev, P.N. Butenko, S.I. Stepanov, A. I. Pechnikov, M.P. Scheglov, E.V. Chernikov, Hydrogen sensors based on Pt/ α -Ga₂O₃/Sn/Pt structures, *Sensor. Actuator. B Chem.* 364 (2022), 131904, <https://doi.org/10.1016/J.SNB.2022.131904>.
- [135] M. Ali, N. Tiri, Z.H. Yamani, Role of defects and dopants in zinc oxide nanotubes for gas sensing and energy storage applications, *Int. J. Energy Res.* 44 (2020) 10926–10936, <https://doi.org/10.1002/ER.5656>.
- [136] S. Nakagomi, T. Sai, Y. Kokubun, Hydrogen gas sensor with self temperature compensation based on β -Ga₂O₃ thin film, *Sensor. Actuator. B Chem.* 187 (2013) 413–419, <https://doi.org/10.1016/j.snb.2013.01.020>.
- [137] M. Fleischer, L. Höllbauer, H. Meixner, Effect of the sensor structure on the stability of Ga₂O₃ sensors for reducing gases, *Sensor. Actuator. B Chem.* 18 (1994) 119–124, [https://doi.org/10.1016/0925-4005\(94\)87069-1](https://doi.org/10.1016/0925-4005(94)87069-1).
- [138] Z. Li, S. Yan, Z. Wu, H. Li, J. Wang, W. Shen, Z. Wang, Y.Q. Fu, Hydrogen gas sensor based on mesoporous In₂O₃ with fast response/recovery and ppb level detection limit, *Int. J. Hydrogen Energy* 43 (2018) 22746–22755, <https://doi.org/10.1016/J.IJHYDENE.2018.10.101>.
- [139] Y.L. Wu, Q. Luan, S.J. Chang, Z. Jiao, W.Y. Weng, Y.H. Lin, C.L. Hsu, Highly sensitive β -Ga₂O₃ nanowire nanowires isopropyl alcohol sensor, *IEEE Sensor. J.* 14 (2014) 401–405, <https://doi.org/10.1109/JSEN.2013.2283885>.
- [140] L. Song, L. Yang, Z. Wang, D. Liu, L. Luo, X. Zhu, Y. Xi, Z. Yang, N. Han, F. Wang, Y. Chen, One-step electrospun SnO₂/Mo_x heterostructured nanomaterials for highly selective gas sensor array integration, *Sensor. Actuator. B Chem.* 283 (2019) 793–801, <https://doi.org/10.1016/j.snb.2018.12.097>.
- [141] Z. Wei, M.K. Akbari, Z. Hai, R.K. Ramachandran, C. Detavernier, F. Verpoort, E. Kats, H. Xu, J. Hu, S. Zhuiykov, Ultra-thin sub-10 nm Ga₂O₃-WO₃ heterostructures developed by atomic layer deposition for sensitive and selective C₂H₅OH detection on ppm level, *Sensor. Actuator. B Chem.* 287 (2019) 147–156, <https://doi.org/10.1016/j.snb.2019.02.046>.
- [142] M. Krawczyk, P. Suchorska-Woźniak, R. Szukiewicz, M. Kuchowicz, R. Korbutowicz, H. Teterycz, Morphology of Ga₂O₃ nanowires and their sensitivity to volatile organic compounds, *Nanomatериалы* 11 (2021) 1–19, <https://doi.org/10.3390/nano11020456>.
- [143] R. Pilliadugula, N.G. Krishnan, Effect of pH dependent morphology on room temperature NH₃ sensing performances of β -Ga₂O₃, *Mater. Sci. Semicond. Process.* 112 (2020), 105007, <https://doi.org/10.1016/j.mssp.2020.105007>.
- [144] R. Pilliadugula, N. Gopalakrishnan, Room temperature ammonia sensing performances of pure and Sn doped β -Ga₂O₃, *Mater. Sci. Semicond. Process.* 135 (2021), 106086, <https://doi.org/10.1016/J.MSSP.2021.106086>.
- [145] P.L. Chen, I.P. Liu, W.C. Chen, J.S. Niu, W.C. Liu, Study of a platinum nanoparticle (Pt NP)/amorphous In-Ga-Zn-O (A-IGZO) thin-film-based ammonia gas sensor, *Sensor. Actuator. B Chem.* 322 (2020), 128592, <https://doi.org/10.1016/J.SNB.2020.128592>.
- [146] H. Okada, A. Naruse, Y. Furukawa, A. Wakahara, Study of electrical response in Pt/GaN Schottky barrier diode to CO gas for high temperature gas sensor, *Jpn. J. Appl. Phys.* 50 (2011), 01AD08, <https://doi.org/10.1143/JJAP.50.01AD08/XML>.
- [147] H.W. Zan, C.H. Li, C.C. Yeh, M.Z. Dai, H.F. Meng, C.C. Tsai, Room-temperature-operated sensitive hybrid gas sensor based on amorphous indium gallium zinc oxide thin-film transistors, *Appl. Phys. Lett.* 98 (2011), 253503, <https://doi.org/10.1063/1.3601488>.
- [148] C. Sun, J. Shao, Z. Wang, H. Liu, Z. Li, H. Zhang, T. Bai, Y. Sun, L. Guo, G. Pan, X. Yang, CuO-sensitized amorphous ZnSnO₃ hollow-rounded cubes for highly sensitive and selective H₂S gas sensors, *Sensor. Actuator. B Chem.* 362 (2022), 131799, <https://doi.org/10.1016/J.SNB.2022.131799>.
- [149] P.P. Gauns Dessai, A.K. Singh, V.M.S. Verenkar, Mn doped Ni-Zn ferrite thick film as a highly selective and sensitive gas sensor for Cl₂ gas with quick response and recovery time, *Mater. Res. Bull.* 149 (2022), 111699, <https://doi.org/10.1016/J.MATERESBULL.2021.111699>.
- [150] K. Liu, M. Sakurai, M. Aono, Enhancing the humidity sensitivity of Ga₂O₃/SnO₂ core/shell microribbon by applying mechanical strain and its application as a flexible strain sensor, *Small* 8 (2012) 3599–3604, <https://doi.org/10.1002/SMLL.201201028>.
- [151] K. Liu, M. Sakurai, M. Aono, One-step fabrication of β -Ga₂O₃-amorphous-SnO₂ core-shell microribbons and their thermally switchable humidity sensing properties, *J. Mater. Chem.* 22 (2012) 12882–12887, <https://doi.org/10.1039/c2jm32230g>.
- [152] Y.M. Juan, S.J. Chang, H.T. Hsueh, T.C. Chen, S.W. Huang, Y.H. Lee, T.J. Hsueh, C.L. Wu, Self-powered hybrid humidity sensor and dual-band UV photodetector fabricated on back-contact photovoltaic cell, *Sensor. Actuator. B Chem.* 219 (2015) 43–49, <https://doi.org/10.1016/J.SNB.2015.05.020>.
- [153] D. Wang, Y. Lou, R. Wang, P. Wang, X. Zheng, Y. Zhang, N. Jiang, Humidity sensor based on Ga₂O₃ nanorods doped with Na⁺ and K⁺ from GaN powder, *Ceram. Int.* 41 (2015) 14790–14797, <https://doi.org/10.1016/J.CERAMINT.2015.07.211>.
- [154] S. Nakata, M. Shiomi, Y. Fujita, T. Arie, S. Akita, K. Takei, A wearable pH sensor with high sensitivity based on a flexible charge-coupled device, *Nat. Electron.* 111 (1) (2018) 596–603, <https://doi.org/10.1038/s41928-018-0162-5>.
- [155] C.W. Hung, K.W. Lin, R.C. Liu, Y.Y. Tsai, P.H. Lai, S.I. Fu, T.P. Chen, H.I. Chen, W. C. Liu, On the hydrogen sensing properties of a Pd/GaAs transistor-type gas sensor in a nitrogen ambience, *Sensor. Actuator. B Chem.* 125 (2007) 22–29, <https://doi.org/10.1016/J.SNB.2007.01.027>.
- [156] H.X. Yu, C.Y. Guo, X.F. Zhang, Y.M. Xu, X.L. Cheng, S. Gao, L.H. Huo, Recent development of hierarchical metal oxides based gas sensors: from gas sensing performance to applications, *Adv. Sustain. Syst.* (2022), <https://doi.org/10.1002/ADSU.202100370>.
- [157] Z. Fang, X. Shen, Z. Wu, T.Y. Zhang, Improved InGaN/GaN quantum wells on treated GaN template with a Ga-rich GaN interlayer, *Phys. Status Solidi A* 212 (2015) 2205–2212, <https://doi.org/10.1002/PSSA.201532246>.
- [158] Z. Wu, X. Shen, H. Xiong, Q. Li, J. Kang, Z. Fang, F. Lin, B. Yang, S. Lin, W. Shen, T.Y. Zhang, Improved interface quality and luminescence capability of InGaN/GaN quantum wells with Mg pretreatment, *Appl. Phys. Mater. Sci. Process* 122 (2016) 1–10, <https://doi.org/10.1007/S00339-016-9661-2/FIGURES/11>.
- [159] Z. Wu, X. Shen, C. Liu, K. Li, W. Shen, J. Kang, Z. Fang, In situ asymmetric island sidewall growth of high-quality semipolar (112) GaN on m-plane sapphire, *CrystEngComm* 18 (2016) 5440–5447, <https://doi.org/10.1039/C6CE00878J>.
- [160] Z. Wu, P. Song, T. Shih, L. Pang, L. Chen, G. Lin, D. Lin, C. Li, R. Liu, W. Shen, J. Kang, Z. Fang, In situ site-specific gallium filling and nanograin growth for blocking of threading defects in semipolar (112) GaN, *Cryst. Growth Des.* 17 (2017) 4687–4693, https://doi.org/10.1021/ACS.CGD.7B00584/ASSET/IMAGES/MEDIUM/CG-2017-00584N_0010.GIF.
- [161] X. Shen, Z. Wu, J. Li, J. Kang, Z. Fang, Phosphor-free white emission from InGaN quantum wells grown on in situ formed submicron-scale multifaceted GaN stripes, *J. Alloys Compd.* 775 (2019) 752–757, <https://doi.org/10.1016/J.JALCOM.2018.09.293>.
- [162] Z. Wu, Z. Jiang, S. Lu, J. Li, R. Liu, J. Kang, Z. Fang, Semipolar (112 $\bar{2}$) GaN films improved by in situ SiN_x pretreatment of m-sapphire substrate surface, *Phys. Status Solidi A* 216 (2019), 1900001, <https://doi.org/10.1002/PSSA.201900001>.
- [163] Z. Wu, T. Shih, J. Li, P. Tian, R. Liu, J. Kang, Z. Fang, Improved semipolar green InGaN/GaN quantum wells on asymmetrically grown (112) GaN templates and their correlations, *CrystEngComm* 20 (2018) 2053–2059, <https://doi.org/10.1039/C8CE00151K>.
- [164] Z. Wu, S. Lu, P. Yang, P. Tian, L. Hu, R. Liu, J. Kang, Z. Fang, Green-amber emission from high indium content InGaN quantum wells improved by interface modification of semipolar (112) GaN templates, *CrystEngComm* 21 (2019) 244–250, <https://doi.org/10.1039/C8CE01648H>.
- [165] E. Chikoidze, A. Fellous, A. Perez-Tomas, G. Sauthier, T. Tchelidze, C. Ton-That, T.T. Huynh, M. Phillips, S. Russell, M. Jennings, B. Berini, F. Jomard, Y. Dumont, P-type β -gallium oxide: a new perspective for power and optoelectronic devices, *Mater. Today Phys.* 3 (2017) 118–126, <https://doi.org/10.1016/J.MTPHYS.2017.10.002>.
- [166] C. Ma, Z. Wu, Z. Jiang, Y. Chen, W. Ruan, H. Zhang, H. Zhu, G. Zhang, J. Kang, T.-Y. Zhang, J. Chu, Z. Fang, Exploring the feasibility and conduction mechanisms of P-type nitrogen-doped β -Ga₂O₃ with high hole mobility, *J. Mater. Chem. C* 10 (2022) 6673–6681, <https://doi.org/10.1039/DITC05324H>.